International Geology Review, Vol. 48, 2006, p. 1087–1112.

Heterogeneity of a Plume Axis: Bulk-Rock Geochemical Evidence from Picrites and Basalts in the Emei Large Igneous Province, Southwest China

HOU ZENGQIAN,[1]

Institute of Geology, Chinese Academy of Geological Sciences, Beijing 100037, People's Republic of China

LU JIREN, AND LIN SHENGZHONG

Institute of Mineral Resources, Chinese Academy of Geological Sciences, Beijing 100037, People's Republic of China

Abstract

In order to document the chemical characteristics of sources of a continental flood basalt (CFB) and to understand its origin, we studied four typical picrite-basalt flows and three picritic intrusions in the Emeishan picrite-cluster field (5×10^4 km^2 area), located in the southwestern part of the Emei large igneous province. Major and trace elements, and Sr-Nd-Pb isotopic compositions, are reported for picrites and associated basalts in the picrite-cluster field, regarded as the axial area of the Emei mantle plume. These rocks exhibit a range of MgO contents (4.2–27.2%), variable degrees of LREE enrichment (La_N/Yb_N = 2.7–29.0), and heterogeneous isotopic ratios ($\varepsilon_{Nd(t)}$ = 4.84 to –4.00; initial $^{87}Sr/^{86}Sr$ = 0.7023–0.7064; $^{206}Pb/^{204}Pb$ = 18.034–20.641). Nd, Sr, and Pb isotopic covariations are similar to at least three groups of the picrites and basalts. Ontong Java-like lavas yielded low $(^{87}Sr/^{86}Sr)_i$ (<0.7045), high $\varepsilon_{Nd(t)}$ (>2.5), and the lowest $(Ce/Yb)_N$ (~4), La/Sm (~3), Th/Nb (~0.75), La/Nb (~0.85), and Ba/Nb (~8) ratios, suggesting a focus zone (FOZO)–like mantle source. Cook-Austral–like lavas have high $^{206}Pb/^{204}Pb$ (>19.0), low $(^{87}Sr/^{86}Sr)_i$ (<0.7045), and high Sm/Yb (>4), Nb/Y (>1) and Zr/Y (>8), similar to the HIMU component. Heard-like lavas yielded high $(^{87}Sr/^{86}Sr)_i$ (0.7044 ~ 0.7060), low $\varepsilon_{Nd(t)}$ (1.7 to –3.0), $^{206}Pb/^{204}Pb$ (18.75–18.03) and $^{208}Pb/^{204}Pb$ (37.8–39.0), and high $(Ce/Yb)_N$ (>10), Ba/Nb (>30), and Th/Nb (>0.1), which might be explained by mixing of picritic magmas from the plume with lamproitic melt from continental lithospheric mantle. Three samples outside the three groups have Sr-Nd isotopic signatures similar to EM I, and high Th/Nb (>0.2), La/Nb (>1.5), and low Nb/U (<25), suggesting a pelagic sediment source component. The picritic intrusives have low $\varepsilon_{Nd(t)}$ (0.32–0.59), intermediate $(^{87}Sr/^{86}Sr)_i$ (0.7037–0.7042), very high Th/Nb (0.11–0.20), and low Nb/U (<25), implying minor crustal assimilation. The trace elements and Sr-Nd-Pb isotope geochemistry of the Emei picrites and associated basalts reflect processes involving: (1) partial melting of a heterogeneous, eclogite-bearing source to produce picritic magmas; then (2) mixing with small amounts of melt from the continental lithospheric mantle; and (3) crustal assimilation during picritic magma ascent. The heterogeneity of this source is related to recycling of subducted oceanic crust and associated sediments into the deep upper mantle.

Introduction

STUDIES ON OCEANIC basalts, especially on oceanic island basalt (OIB), have recognized several geochemical mantle end-members—i.e., depleted mantle (DMM), enriched mantle (EM I and EM II), high-mantle (HIMU), focus zone (FOZO), and common (C) and primitive helium mantle end-members (PHEM) (Zindler and Hart, 1986; Hart, 1988; Hart et al., 1992; Farley et al., 1992; Hanan and Graham, 1996). An early proposed hypothesis that the HIMU and EM sources are to be regarded as recycled oceanic crust and associated sediments is widely supported by recent studies, especially Re-Os isotope studies (Hofmann and White, 1982; Weaver, 1991; Chauvel et al., 1992; Hauri and Hart, 1993; Reiberg et al., 1993; Rogers et al., 2000; Hofmann, 1997). However, the genesis of continental flood basalts (CFB) is still debated because generation of CFBs is related to both continental lithospheric mantle (CLM) and crust. Some researchers argued that CFBs were directly derived from lithospheric mantle (Carlson, 1984; Hawkesworth et al., 1988; Hergt et al., 1991; Gallagher and

[1]Corresponding author: houzengqian@126.com

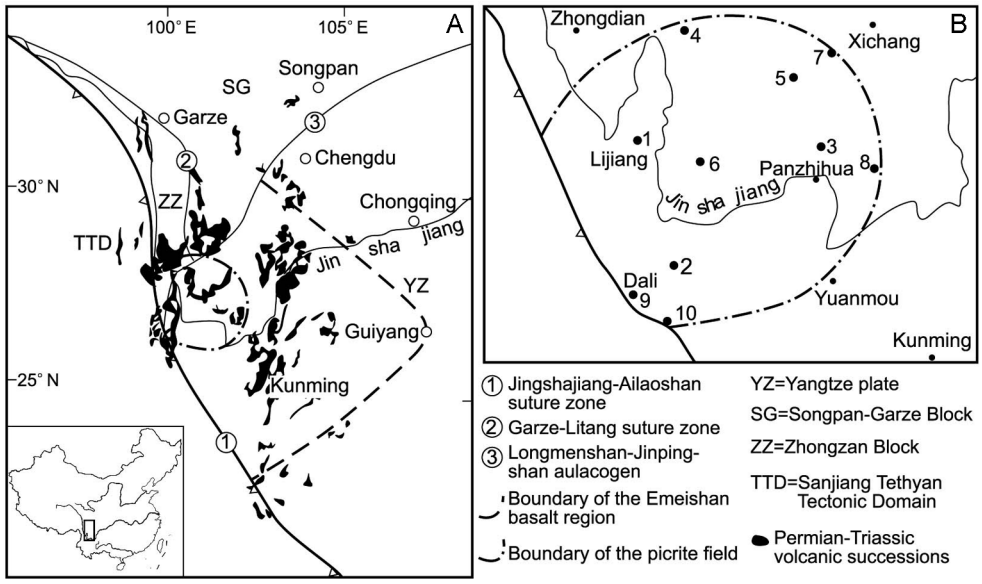

FIG. 1. Distribution of Emei basalts and picrites, and relationships to the tectonic framework. A. Simplifed geologic map of the Emei large igneous province, showing distribution of Permian–Triassic volcanic successions. B. Picrite field and sampling locations corresponding to the axial area of the plume: 1 = Lijiang; 2 = Binchuan; 3 = Ertan; 4 = Yongning; 5 = Bailinshan; 6 = Yongsheng; 7 = Pingchuan; 8 = Miyi; 9 = Dali, induding Wulongba, Puhe, and Hanyi.

Hawkesworth, 1992; Lightfoot et al., 1993; Turner and Hawkesworth, 1995); others pointed out that this scenario would be unlikely to explain the source of heat and rate of magma generation (Menzies, 1992; Coffin and Eldholm, 1994; White and McKenzie, 1995; Campbell, 1998). Although it is mostly accepted that CFBs are derived from a mantle plume originating from the thermal boundary layers (2900 km or 660 km), and with the same source as ocean-island basalt, the problem of how crustal contamination and plume-derived melt/lithosphere mantle interactions affected CFB compositions is still debated.

The picrite-basalt association from the CFB province is regarded as a melting product of the mantle plume axis, and can be compared geochemically with OIB (Campbell and Griffiths, 1990). The major difference is that the former is a product of the plume head, whereas the latter is that of the plume tail, which probably formed during the earlier and later phases of plume magma activity, respectively. Melting in the plume head generates high-temperature picritic magmas derived from its axial zone, and provide geochemical information on various mantle end-members and/or their mixtures that are represented in OIBs.

The Emeishan CFBs dominate the Emei large igneous province (ELIP), in which a picrite-cluster field is developed (Fig. 1A). Lin (1981) and Zhang et al. (1988) studied the petrology of the picrite-basalt association in this field, the petrogenesis of which was attributed to activity of a Permian mantle plume by several other researchers (Chung and Jahn, 1995; Lu, 1996; Chung et al., 1998; Hou et al., 1999; Song et al., 2001a, 2001b; Xu et al., 2001). However, the nature and geochemistry of the source in relation to a mantle plume are not well constrained, and the relative contribution of the plume source, CLM, and continental crust in generation of the Emeishan CFBs is less wellunderstood. Our data, combined with that reported previously, indicate that the ELIP lavas probably were derived from the melting of a heterogeneous, eclogite-bearing plume, in which a FOZO component from the deep mantle mixed with oceanic crust and associated sediments that had recycled deeply into the mantle. To test this hypothesis, our study has surveyed in detail five picritic and four basaltic districts within the picrite-cluster field (Fig. 1B) in the ELIP, and analyzed major and trace elements as well as Sr, Nd, and Pb isotope compositions of the picrites and basalts.

Geological Setting

Stratigraphy and time of eruption of volcanic seqeunce

The Emeishan CFB dominates the Emei large igneous province (ELIP), with an area of about 5×10^5 km^2 (Fig. 1). The geology of the ELIP has been described by many researchers (see Xu et al., 2001), and so only a few geological aspects are emphasized here. The Yangtze basement is composed mainly of Mesoproterozic metamorphic rocks, cropping out along the western margin of the craton. Phanerozoic cover strata are dominated by a Silurian–Triassic clastic-carbonate sequence and a Permian continental flood basalt. The CFB succession uncomformably overlies an erosion surface on the Middle Permian Maokou limestone. In turn the CFB is comformably covered by the Upper Permian Longtan or Xuanwei coal-bearing formations, suggesting that rapid regional uplift was followed by a strong eruptive event of mafic volcanism coeval with or older than the Longtainian at 253–258 Ma (Xu et al., 2001). The main eruptive age is estimated to be 259 ± 2 Ma (Lu, 1996; Song et al., 2001b; Courtillot et al., 1999), which has recently been supported by a laser microprobe $^{40}Ar/^{39}Ar$ age of ~259 Ma for pyroxene phenocrysts in the CFB (Hou et al., unpubl. data). This implies regional uplift, subsequent basement subsidence, and associated emplacement of large-volume mafic magmas over a short duration (<2 Ma), attributed to Permian mantle plume activity (Lu, 1996; Chung et al., 1998; Hou et al., 1999; Song et al., 1999).

The Emeishan CFB is quite variable in thickness, from 5400 m to 200 m from west to east, with an average thickness of about 700 m and a minimum estimated volume of 0.3×10^6 km^3 (Xu et al., 2001). Erupted rocks vary from picrite-dominated and picrite-basalt associations to tholeiitic flood basalt successions. Picritic lavas and associated intrusions mainly cluster in the western part of the ELIP (Fig. 1A), and are present in an area of 5×10^4 km^2 characterized by the maximum thickness of flows, accounting approximately for 10% of the ELIP.

Picrite-bearing volcanic sequence

At least four picrite-bearing volcanic sequences have been recognized in the picrite-cluster field—Lijiang, Binchuan, Panzhihua, and Bailingshan—which developed around a >300 m thick flood basalt area at Yongsheng, in the center of the field (Fig. 1B). The subvolcanic picrites or picritic basalts occur as dikes sills, or stocks scattered around the field; only three bodies (Wulongba, Hanyi, and Puhe) near Dali city were surveyed in this study. These picrite-bearing sequences are variable in thickness and rock association. At Binchuan, a 5384 m thick volcanic section consists of basal basalt and basaltic pyroclastics, a lower basalt-picrite suite, a middle basalt-picrite suite, and upper massive, porphyitic basalt flows with a picrite layer. This volcanic sequence is dominated by thick basalt flows, with thin lava flows of picrites intercalated at three levels (Xu et al., 2001). Similarly, at Bailinshan, a >300 m thick volcanic sequence consists of a thick basaltic lava flow and an underlying thin-layered picritic flow. By contrast, at Lijiang, a volcanic sequence is dominated by picritic lavas with minor thin-layered basalt flows in a 200 m thick section. At Ertan, picritic lava flows are intercalated with basaltic lavas, and occur mainly in the lower to middle parts of a 1000 m thick section, consisting of a picritic-basaltic succession and an overlying trachytic-rhyolitic succession (Chung and Jahn, 1995). Independent basaltic flows are located mainly outside the picrite-cluster field (Fig. 1B), and extend outward for 300 km as flows with thicknesses varying from 100 m to 800 m (Lin, 1981).

Picritic rocks are aphyric and phyric, with olivine and clinopyroxene phenocrysts set in a groundmass of clinopyroxene, olivine, mafic microlite, and minor plagioclase + magnetite. Olivine phenocrysts have a limited range of Fo values of 92–94% (Zhang and Wang, 2003a, 2003b). Basaltic lavas associated with picrite are typically tholeiitic and can be divided into two groups, i.e., low-Ti and high-Ti basalts (Xu et al., 2001). High-Ti basalts are widely intercalated with picritic lavas, whereas lower-Ti basalts occur only in the Binchuan sequence. The independent lavas are dominated by high-Ti tholeiitic basalts with minor alkaline basalts (e.g., at Yongning).

Analytical Methods

Major and trace elements of bulk-rock samples were analyzed in the National Research Center of Geoanalysis, Chinese Academy of Geological Sciences (CAGS, Beijing). Analyzed samples for major elements were fused with lithium metaborate and analyzed with inductively coupled plasma emission spectrometer (ICP-AES, JA-1160). Samples for rare-earth elements (REEs) were fused with Na_2O_2, and then REEs were separated and concentrated,

and analyzed with ICP-AES. Some samples with low REE contents were analyzed with an inductively coupled plasma mass spectrometer (ICP-MS). The samples for Nb, Ta, Zr, and Hf were fused with Na_2O_2, eluted with H_2O and acidified, and analyzed with ICP-MS. The samples for the other trace elements were dissolved in a mixture of HCl–HNO_3–HF–$HClO_4$, and analyzed with ICP-AES or ICP-MS.

Sr and Nd isotopes were determined with a VG354 mass spectrometer in the Isotope Department of the Institute of Geology, Chinese Academy of Sciences (CAS, Beijing). The powdered samples were dissolved in a mixture of HF and $HClO_4$ in Teflon capsules under low-temperature, and pure Rb, Sr, Sm, and Nd were separated by using AG50W×8(H^+) cation exchange columns and P507 extract-drip resin. Total procedure blanks for Rb-Sr are about 200–500 pg. Correction for mass fractionation was made by normalizing to $^{86}Sr/^{88}Sr$ = 0.1194. Measured mean $^{87}Sr/^{86}Sr$ for the NBS 987 standard is 0.71025 ± 16. Blank levels for Sm-Nd are about 50 pg. Correction for mass fractionation was made by normalizing to $^{146}Nd/^{144}Nd$ = 0.7219. Measured mean $^{143}Nd/^{144}Nd$ for the BCR-1 Nd standard is 0.512626 ± 9.

Pb isotope analyses were carried out with a MAT261 multi-collector mass spectrometer in the Laboratory for Isotope Geology, CAGS (Beijing). The powdered samples were dissolved in a mixture of HF and HNO_3, and Pb was separated by conventional ion exchange column. The total blank for Pb is typically 1 ng. The instrument was calibrated against standard NBS981.

Results

Major elements

Volcanic rocks in the picrite-cluster field show a very wide variation in major element compositions (Fig. 2). The picritic rocks are dominated by picrite with minor picritic basalts, having MgO contents of 13.6–27.3 wt %, whereas basaltic rocks are dominated by tholeiitic basalts with variable MgO contents between 4.2 and 11.2 wt% (Table 1).

Correlations between MgO and SiO_2, Al_2O_3, Ni, and Cr contents (Fig. 2) indicate that the picritic rocks underwent variable degrees of crystal fractionation. Based on the Fo value (92–94%) of olivine phenocryst (Zhang and Wang, 2003a, 2003b), contents of MgO and FeO, and abundances of Cr and Ni, the picrites with MgO of 25–16 % can be considered as primary magmas, whereas picritic rocks with MgO >25% and <16% probably represent olivine-accumulated and more evolved products of the primary magmas, respectively (Zhang et al., 2003). Olivine-accumulated picrites are represented by the Lijiang picrites, which yielded high contents of MgO (25.2–27.3 wt%), and high abundances of Cr (up to 2900 ppm) and Ni (>730 ppm), whereas evolved picrites dominate the Bailingshan and Binchuan lavas, which have lower MgO contents of 13.6–15.4 wt% and lower abundances of Ni <620 ppm and Cr <2000 ppm (Table 1). Primary picrites occur in all four volcanic districts, and are characterized by much high Ni (455–1100 ppm) and Cr (1100–2600 ppm) abundances.

Most basaltic samples are tholeiitic, except for three samples from the Yongning district (LY-06, 07, and 08), which are strongly alkaline basanite–tephrite and potassic trachybasalt with normative olivines (Ol) of 23.1 wt% and 3.4 wt%, respectively. The MgO contents of all basaltic samples are usually less than 11.2 wt%, and five of them are less than 6 wt% (5.6–3.5 wt%), suggesting a strong differentiation of basaltic magma. TiO_2 content ranges from 1 wt% to 4 wt%, but displays a transitional variation (Fig. 2). There are passive correlations between MgO and SiO_2, Al_2O_3, TiO_2, and T_{FeO} for basaltic and picritic rocks but only from two districts (Ertan and Lijiang), which indicates that more evolved basalts were derived from parental picritic magmas by crystallization differentiation (Chung and Jahn, 1995).

Rare-earth elements

Picrites and associated basalts in the ELIP exhibit variable LREE enrichment, with $(La/Yb)_N$ ranging from 2.7 to 29.0 without any Eu anomaly (Fig. 3). At Ertan, the low-level picrite (EM-70) has the lowest Yb (0.98 ppm) and the highest La (42 ppm) abundances; high-level picrites have relatively high Yb (1.4–1.5 ppm) but the lowest La (8.4–15.0 ppm) with $(La/Yb)_N$ of 4.1–6.9, whereas middle-level picrites have a Yb range of 1.3–1.6 ppm and intermediate La abundances (25.7–31.1 ppm) with a wide $(La/Yb)_N$ range of 19.7–29.0 (Xu et al., 2001, Table 1). Associated basalts generally yield higher REE abundances but similar REE patterns to those of picrites (Fig. 3A). Similarly, at Binchuan, all picrites display a narrow Yb range of 0.9–1.5 ppm, but have much more variable LREE abundances (4.4–31.3 ppm). The high-level picrite (EM-43) has the lowest La abundance (4.4 ppm) with $(La/Yb)_N$ of 2.7 (Xu et al., 2001), middle-level picrite

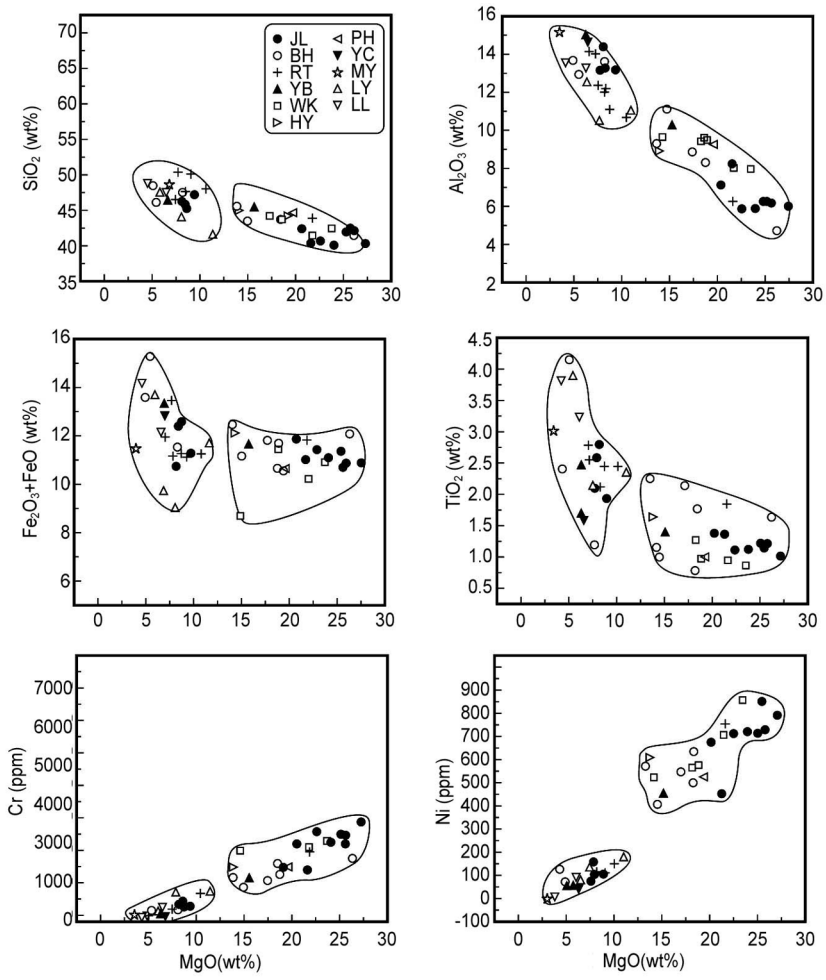

FIG. 2. MgO content plotted against abundances of some major element oxides, Cr and Ni, showing the composition and the relations of picrite and basalt in the ELIP. Symbols in inset are as follows: JL = Lijiang; BH = Binchuan; RT = Ertan; LY = Yongning; YB = Bailinshan; LL = Yongsheng; YC = Pingchuan; MY = Miyi; WK = Wulongba; PH = Puhe; HY = Hanyi.

(BH-10) has the highest La abundance (39.9 ppm) with high $(La/Yb)_N$ of 18.2, whereas the low-level picrites (BH-15, -17, -19, 20) yielded intermediate La abundances of 20.4–31.3 ppm with $(La/Yb)_N$ of 12.8–17.5 (Fig. 3B, Table 1). Associated basalts have relatively high Yb abundance (2.2–3.2 ppm) and a range of $(La/Yb)_N$ varying from 6.1 to 25.8. The Lijiang picrites display a limited variation in REE abundance and $(La/Yb)_N$ (5.9–11.8). Their Yb abundances (0.6–1.1 ppm) are similar to, but La abundances are much lower (8.5–12.4 ppm) than those of lower-level picrite at Ertan. Intercalated basalts yielded identical REE patterns to the picrites (Fig. 3C), suggesting a genetic connection, such as crystal fractionation.

Two groups of picritic intrusives occur at Wulongba—i.e., low-La and high-La picritic rocks (Fig. 3D). The former has lower La abundances (5.0–5.8 ppm) and $(La/Yb)_N$ ratios (2.7–4.1) similar to high-level picritic lavas (BZ-9, EM-43) at Binchuan. The latter have relatively high La abundance (10.8 ppm) and $(La/Yb)_N$ ratios (5.4) identical to those of picritic dikes at Puhe (La = 9.8 ppm) and Hanyi (La = 14.9 ppm), and of picritic basalt at

TABLE 1. Major- and Trace-Element Compositions of Representative Samples from the Emeishan CFB Province

Location:	Lijiang												Binchuan	
Sample:	JL-3	JL-4	JL-13	JL-17	JL-18	JL-20	JL-21	JL-23	JL-26	JL-28	JL-29	JL-31	BH-7	EM-52
Rock:[1]	P	P	B	P	P	P	B	P	B	B	P	P	B	B
							wt%							
SiO_2 %	42.09	41.95	47.08	41.94	40.46	40.33	45.69	40.27	46.10	45.21	42.16	39.96	45.82	48.61
TiO_2	1.19	1.21	1.94	1.23	1.14	1.37	2.57	1.04	2.08	2.76	1.39	1.14	4.09	3.65
Al_2O_3	6.12	6.10	13.02	6.16	5.78	8.13	13.15	5.94	14.22	12.32	7.04	5.76	12.73	12.69
Fe_2O_3	3.08	3.52	3.90	4.20	5.17	2.81	5.20	3.17	6.80	5.94	5.50	4.47	5.51	14.89
FeO	7.65	7.34	7.36	7.16	6.26	8.24	7.15	7.73	3.93	6.61	6.36	6.63	9.63	
MnO	0.16	0.16	0.26	0.17	0.21	0.18	0.20	0.17	0.55	0.22	0.22	0.20	0.20	0.19
MgO	25.52	25.73	9.13	25.18	22.57	21.51	8.10	27.23	7.81	8.29	20.44	23.93	5.21	5.42
CaO	7.28	6.73	10.30	6.33	7.93	7.80	9.94	6.22	10.02	10.51	7.71	6.44	7.84	10.26
Na_2O	0.51	0.44	2.76	0.50	0.25	0.37	2.47	0.32	2.49	2.92	0.59	0.24	3.37	2.03
K_2O	0.14	0.14	0.88	0.12	0.02	0.03	1.59	0.18	0.37	0.66	0.12	0.03	1.47	0.50
P_2O_5	0.11	0.11	0.17	0.1	0.1	0.1	0.28	0.12	0.63	0.29	0.13	0.1	0.47	0.36
LOI	4.96	5.70	2.34	5.96	9.62	8.00	2.28	6.72	4.66	3.04	7.64	9.98	2.82	1.46
Total	98.81	99.13	99.14	98.95	99.41	98.77	98.62	99.11	99.66	98.77	99.30	98.78	99.16	100.06
							ppm							
Cs	0.3	0.3	0.3	0.5	0.3	0.4	0.3	0.4	0.4	0.2	0.4	0.4	0.5	
Rb	4.1	7.2	17.0	5.8	3.0	2.5	27.0	8.6	10.0	11.0	4.7	4.2	27.0	10
Sr	118	83	497	83	94	68	1100	54	596	486	81	77	706	541
Ba	207	156	601	140	107	125	1100	150	449	341	154	109	570	221
Sc	15.03	20.50	27.22	20.80	24.03	24.21	21.96	17.66	19.72	26.05	22.47	19.04	25.10	
V	175	173	335	172	172	217	288	154	240	312	193	153	436	486
Cr	2500	2200	278	2500	2600	1400	442	2900	392	297	2200	2300	114	82
Co	45	42	46	42	43	62	41	42	45	41	41	40	42	48
Ni	855	731	109	717	712	455	164	794	86	112	674	724	75	‘102
Y	8.13	10.78	16.10	11.18	10.20	13.06	18.49	8.76	19.97	21.03	10.79	9.67	36.84	36
Zr	86	88	126	79	84	94	190	78	145	198	92	97	274	242
Hf	2.3	2.3	3.6	2.1	2.1	2.3	4.6	1.9	3.4	5.0	2.4	2.5	7.4	6.6
Nb	12	11	18	12	10	10	31	12	42	26	14	11	38	33
Ta	1.6	1.6	1.5	1.4	1.1	0.9	2.8	1.0	2.7	1.9	1.3	0.9	2.6	2.1
U	0.4	0.4	0.4	0.3	0.3	0.3	0.7	0.3	0.6	0.6	0.4	0.2	1.1	0.9
Th	1.4	1.4	1.6	1.4	1.1	1.2	3.1	1.1	3.1	2.5	1.4	1.0	4.4	3.9
Pb	3.3	4.1	7.7	11	1.9	5.0	4.7	9.4	4.6	18	2.8	2.1	6.9	
							ppm							
La	10.26	10.60	13.38	12.40	8.50	9.28	20.82	9.98	23.89	24.69	11.37	8.52	37.88	34.4
Ce	20.34	20.64	26.75	24.01	17.42	19.23	41.07	18.71	43.57	49.48	22.30	17.32	73.93	79.1
Pr	2.60	2.53	3.43	2.97	2.21	2.46	5.08	2.35	5.61	6.25	2.85	2.25	9.76	
Nd	11.25	11.79	15.77	13.75	10.29	11.92	22.24	10.16	22.78	27.67	12.28	10.17	40.14	39.7
Sm	2.88	2.86	4.18	3.39	2.70	3.16	5.37	2.31	5.43	6.85	3.09	2.55	10.12	9.08
Eu	0.91	0.99	1.43	1.13	0.94	1.12	1.74	0.82	1.82	2.14	1.03	0.88	3.04	2.82
Gd	2.77	2.97	4.71	3.15	2.64	3.24	5.76	2.55	5.06	6.52	3.04	2.64	10.16	
Tb	0.36	0.42	0.54	0.43	0.36	0.44	0.70	0.3	0.67	0.84	0.40	0.37	1.30	1.18
Dy	1.88	2.27	3.49	2.58	2.20	2.81	4.03	1.86	4.00	4.87	2.40	2.06	7.84	
Ho	0.40	0.47	0.69	0.49	0.44	0.55	0.78	0.36	0.80	0.90	0.44	0.42	1.60	
Er	0.72	1.12	1.65	1.29	1.15	1.52	1.87	0.94	2.11	2.36	1.18	1.02	3.95	
Tm	0.1	0.15	0.21	0.16	0.15	0.20	0.24	0.12	0.27	0.27	0.15	0.13	0.56	
Yb	0.59	0.88	1.27	0.87	0.86	1.06	1.48	0.75	1.74	1.58	0.85	0.77	2.96	2.22
Lu	0.1	0.14	0.19	0.13	0.15	0.17	0.24	0.1	0.26	0.21	0.11	0.1	0.49	0.34

Table continues

TABLE 1. *Continued*

Location:	Binchuan												Ertan			
Sample:	BZ-9	EM-43	EM-42	BH-8	BH-10	BH-11	BH-15	BH-17	BZ-26	BH-19	BH-20	RT-29	RT-24	EM-84	EM-83	RT-15
Rock:[1]	B	P	B	Picb	P	B	P	Picb	B	P	P	B	B	B	P	B
								wt%								
SiO_2	48.38	41.86	46.96	43.38	43.62	47.23	44.14	45.34	48.63	43.62	41.39	48.60	47.49	46.95	44.28	46.56
TiO_2	2.12	0.58	4.00	1.03	0.80	1.20	2.14	2.26	3.19	1.78	1.64	2.42	2.12	2.55	1.77	2.76
Al_2O_3	13.92	6.99	12.82	10.95	9.56	13.52	8.79	9.17	13.99	8.20	4.65	13.97	12.01	15.07	9.25	13.86
Fe_2O_3	5.27	11.08	15.99	6.05	5.18	6.61	4.98	6.92	6.71	4.55	6.11	4.58	5.12	13.10	12.78	4.58
FeO	6.29			5.13	5.44	4.89	6.79	5.56	7.62	7.07	5.95	7.40	7.46			8.83
MnO	0.15	0.18	0.21	0.18	0.17	0.18	0.17	0.15	0.23	0.16	0.16	0.21	0.22	0.19	0.17	0.23
MgO	7.32	25.70	5.06	14.66	18.52	8.01	17.37	13.62	4.17	18.60	26.21	6.53	8.33	6.96	15.98	7.11
CaO	12.70	7.30	10.68	11.73	9.66	11.16	8.70	9.42	10.33	8.80	5.83	8.18	10.85	10.12	9.71	10.28
Na_2O	1.66	0.16	2.23	1.01	1.07	1.19	1.40	1.34	2.16	1.15	0.53	3.06	3.01	2.52	1.21	2.68
K_2O	0.29	0.09	0.55	0.36	0.23	2.08	0.70	1.08	0.58	0.58	0.29	2.12	0.74	0.85	0.44	0.42
P_2O_5	0.17	0.12	0.42	0.50	0.31	0.47	0.31	0.33	0.43	0.24	0.25	0.26	0.22	0.28	0.15	0.34
LOI	1.56	5.41	1.04	4.42	4.66	1.86	3.68	3.82	2.20	3.96	6.26	1.74	1.78	0.68	2.67	0.62
Total	100.10	99.47	99.96	99.40	99.22	98.40	99.17	99.01	100.24	98.71	99.27	99.07	99.35	99.26		98.27
								ppm								
Cs	0.15			1.9	1.7	0.5	1.9	1.2	0.22	1.3	1.1	1.3	0.6			0.2
Rb	7.7	5	10	15	9.4	67	22	22	4.4	19	14	59	25	24	12	8.7
Sr	327	68	419	648	417	2200	371	408	471	319	142	658	552	595	148	540
Ba	124	99	219	759	452	4100	594	1200	521	508	298	1400	295	339	172	377
Sc	33.00			26.36	28.44	30.55	21.58	21.05	29.4	22.20	18.42	24.86	32.15			27.05
V	384	132	524	231	190	240	232	248	384	223	160	320	246	344	309	320
Cr	415	2344	98	940	1600	168	1100	1200	41	1300	1800	155	452	169	1717	168
Co	52.9	95	45	59	34	44	67	70	54	69	45	40	46	49	72	45
Ni	143	1160	77	408	502	113	547	572	38	634	1100	89	133	101	828	79
Y	25.00	9	43	18.80	17.04	26.50	15.60	16.00	40.2	15.41	12.39	22.61	19.94	29	21	24.13
Zr	116	34	257	116	75	118	166	176	322	135	152	164	139	196	112	116
Hf	3.19	0.9	6.8	2.6	1.9	2.8	4.3	4.6	7.4	3.4	3.7	4.5	3.7	5.3	2.6	2.9
Nb	11.5	8	34	33	26	42	29	32	43	24	20	25	18	25	14	30
Ta	0.73	0.3	2.1	1.9	1.4	2.2	2.2	2.3	2.8	1.7	1.5	1.9	1.6	1.4	0.6	1.9
U	0.32		0.9	1.6	1.1	1.8	0.9	0.9	1.4	0.8	0.7	0.9	0.8	0.6	0.3	0.3
Th	1.1	0.5	3.9	8.2	6.0	10	3.7	3.8	6.7	3.5	2.4	3.3	2.5	2.8	1.7	5.0
Pb	2.4			11	8.5	14	14	6.2	6.8	6.7	4.4	0.19%	8.0			5.4
								ppm								
La	10.2	4.41	33.70	56.21	39.91	68.08	28.68	31.30	49.4	23.69	20.44	30.53	21.69	27.4	15.3	27.17
Ce	25.00	10.1	74.40	94.59	64.55	111.2	52.33	56.57	107.0	43.89	37.89	56.13	40.90	74.0	32.3	52.70
Pr	4.370			10.82	7.32	12.92	6.67	7.11	13.9	5.39	4.85	7.33	5.23			7.26
Nd	17.60	4.9	45.00	37.35	24.91	41.05	26.36	28.22	54.3	20.91	19.78	28.14	22.18	40.7	19.43	29.97
Sm	4.28	1.28	9.79	7.66	4.98	8.61	6.11	6.37	9.30	4.92	4.83	6.79	5.59	7.46	4.37	7.40
Eu	1.62	0.43	3.10	2.15	1.48	2.41	1.83	1.94	2.82	1.46	1.40	2.08	1.79	2.33	1.25	2.44
Gd	4.28			6.45	4.43	7.10	5.42	5.28	8.48	4.68	3.78	6.56	5.72			6.87
Tb	0.78	0.30	1.36	0.71	0.62	0.97	0.69	0.74	1.31	0.62	0.49	0.74	0.80	0.92	0.57	0.88
Dy	4.67			4.46	3.54	5.70	3.64	3.87	7.23	3.44	2.96	4.92	4.34			5.24
Ho	0.95			0.83	0.69	1.15	0.71	0.72	1.40	0.66	0.60	0.99	0.86			1.06
Er	2.31			2.13	1.85	3.02	1.73	1.86	3.60	1.79	1.60	2.58	2.36			2.74
Tm	0.31			0.27	0.25	0.38	0.22	0.23	0.48	0.24	0.21	0.34	0.28			0.35
Yb	2.17	1.12	3.20	1.47	1.48	2.30	1.22	1.21	3.34	1.25	0.97	1.88	1.64	2.40	1.50	1.99
Lu	0.29	0.16	0.46	0.25	0.22	0.31	0.14	0.15	0.47	0.19	0.15	0.28	0.23	0.33	0.20	0.28

Table continues

TABLE 1. *Continued*

Location	Ertan							Dali						
Sample:	RT-11	EM-79	RT-8	RT-5	RT-3	RT-1	EM-70	WK-02	WK-05	WK-10	WK-12	WK-15	PH-02	HY-02
Rock:[1]	B	P	B	B	B	P	P	Picb	P	P	P	P	P	Picb
							wt%							
SiO_2	50.20	43.90	47.84	48.66	49.98	43.80	45.18	48.56	43.55	44.18	42.41	41.34	44.38	44.69
TiO_2	2.56	1.32	2.44	2.69	2.43	1.88	2.14	1.16	1.29	0.98	0.90	0.98	1.02	1.66
Al_2O_3	12.25	7.73	10.58	11.95	10.99	6.23	6.41	9.60	9.34	9.49	8.01	8.00	9.22	8.85
Fe_2O_3	3.77	13.75	2.75	3.91	3.93	5.48	12.21	2.84	4.67	4.06	4.24	2.64	3.90	6.39
FeO	7.38		8.64	7.31	7.19	6.37		5.88	6.78	6.53	6.63	7.59	6.79	5.76
MnO	0.17	0.20	0.18	0.17	0.16	0.16	0.16	0.15	0.19	0.16	0.16	0.16	0.17	0.15
MgO	7.40	19.19	10.35	8.26	8.72	21.66	19.78	14.46	18.47	19.10	23.63	21.74	19.47	13.93
CaO	9.97	10.30	9.93	8.01	7.71	6.42	9.04	9.70	9.11	8.32	7.03	7.98	8.65	10.00
Na_2O	2.56	0.79	1.06	3.00	2.05	0.72	1.05	1.52	1.27	1.14	0.87	0.16	1.08	1.23
K_2O	1.01	0.74	2.47	2.00	2.41	0.76	0.12	0.17	0.31	0.22	0.20	0.03	0.50	0.50
P_2O_5	0.29	0.09	0.25	0.32	0.36	0.20	0.24	0.18	0.17	0.18	0.11	0.17	0.15	0.20
LOI	1.56	0.49	2.32	2.36	2.84	4.94	2.49	4.24	3.42	4.20	4.96	8.16	3.82	5.86
Total	99.11		98.81	98.64	98.77	98.62		98.46	98.57	98.56	99.15	98.95	99.15	99.22
							ppm							
Cs	0.2		0.2	0.2	0.3	1.9		1.7	3.1	3.9	3.7	1.1	5.3	6.3
Rb	22	21	60	35	46	31	2	5.1	16	17	22	2.7	24	16
Sr	566		515	502	734	281	229	113	170	164	94	23	248	313
Ba	486	113	619	564	619	299	45	158	249	298	151	122	341	383
Sc	26.15		26.92	22.10	21.18	17.61		22.73	23.79	23.62	19.57	16.88	22.67	26.06
V	275	258	290	274	269	219	226	200	197	181	219	250	185	226
Cr	290	1590	705	383	403	2000	1906	2000	1600	1500	2300	2100	1500	1500
Co	40	82	51	43	42	41	73	53	62	61	45	38	64	60
Ni	86	794	160	111	114	750	1004	520	561	574	857	704	529	614
Y	20.75	13	18.75	21.05	22.27	12.87	4.9	14.95	15.86	14.45	12.21	11.44	15.08	15.23
Zr	210	72	209	235	267	169	181	79	106	74	59	64	78	102
Hf	5.0	2.1	4.8	5.6	6.0	3.7	4.9	2.0	2.8	1.8	1.5	1.7	2.0	2.5
Nb	32	9	32	36	41	27	34	5.9	10	5.6	4.6	4.9	8.8	15
Ta	2.0	0.6	2.0	2.4	2.5	1.8	1.9	0.5	0.8	0.6	0.5	0.5	1.1	1.4
U	0.7	0.2	1.2	1.4	1.5	0.9	1.1	0.3	0.4	0.5	0.3	0.5	0.6	0.5
Th	2.8	0.7	5.5	6.7	7.1	3.8	5.3	0.8	1.4	0.7	0.9	0.9	1.9	1.6
Pb	18		10	16	11	16		4.6	5.9	4.8	3.5	2.5	9.2	8.6
							ppm							
La	32.23	8.4	38.97	46.12	49.53	28.30	42.0	5.76	10.77	5.17	5.00	5.50	9.82	14.93
Ce	62.60	19.2	73.50	87.20	93.92	53.96	87.5	11.55	20.73	10.91	9.65	10.87	18.08	29.97
Pr	8.17		9.24	10.93	12.05	6.74		1.63	2.54	1.46	1.42	1.40	2.42	3.84
Nd	32.09	11.53	36.41	43.02	45.49	27.79	41.11	7.48	11.91	7.06	6.61	7.66	9.74	16.50
Sm	7.81	2.82	7.98	9.40	9.92	6.07	7.36	2.65	3.41	2.55	2.38	2.27	2.76	4.20
Eu	2.30	0.85	2.28	2.61	2.66	1.75	1.74	1.01	1.16	0.97	0.82	0.86	0.95	1.37
Gd	7.07		6.65	7.30	7.24	4.50		3.34	3.93	3.45	2.71	2.86	3.01	4.05
Tb	0.84	0.51	0.74	0.83	0.97	0.58	0.90	0.48	0.52	0.50	0.42	0.38	0.54	0.63
Dy	4.69		4.35	4.86	5.19	3.13		2.99	3.29	2.94	2.63	2.43	3.05	3.41
Ho	0.93		0.82	0.86	0.95	0.56		0.63	0.66	0.61	0.53	0.49	0.61	0.64
Er	2.28		2.12	2.32	2.56	1.51		1.62	1.86	1.76	1.42	1.21	1.65	1.69
Tm	0.29		0.26	0.28	0.32	0.17		0.21	0.24	0.23	0.18	0.14	0.22	0.23
Yb	1.64	1.40	1.48	1.66	1.80	0.97	0.98	1.31	1.34	1.31	1.09	0.91	1.38	1.25
Lu	0.24	0.13	0.22	0.23	0.27	0.14	0.13	0.21	0.19	0.20	0.15	0.13	0.21	0.20

Table continues

TABLE 1. *Continued*

Location:	Bailinshan		Pingchuan	Yongsheng				Miyi	Yongning		
Sample:	YB-01	YB-04	YC-04	LL-04	LL-09	DD-11	DD-17	MY-02	LY-06	LY-07	LY-08
Rock:[1]	Picb	B	B	B	B	B	B	B	Bs	Tph	Tb
						wt%					
SiO_2	45.30	46.07	48.53	48.50	47.36	47.83	50.17	51.10	41.33	48.69	43.77
TiO_2	1.40	1.69	1.61	3.79	3.21	3.75	3.62	2.99	2.33	2.44	2.10
Al_2O_3	10.19	14.90	14.54	13.44	13.26	12.93	12.70	15.10	10.98	12.42	10.15
Fe_2O_3	5.02	6.54	2.72	6.44	4.88	7.80	6.94	4.99	3.62	4.13	3.32
FeO	6.56	6.68	10.13	7.68	7.25	6.81	5.59	6.44	8.05	5.60	5.72
MnO	0.17	0.20	0.20	0.22	0.17	0.20	0.18	0.19	0.18	0.14	0.13
MgO	15.38	6.43	6.56	4.24	6.20	4.24	5.18	3.46	11.20	6.60	7.79
CaO	10.20	11.05	8.06	7.96	9.35	9.77	9.23	8.15	12.72	9.78	14.88
Na_2O	1.37	2.34	3.07	3.65	3.24	2.37	2.60	3.80	0.56	1.43	1.28
K_2O	0.11	0.80	1.32	1.22	1.47	1.59	0.51	0.56	2.32	4.82	3.43
P_2O_5	0.14	0.30	0.22	0.55	0.45	0.49	0.39	0.44	0.35	0.40	0.32
LOI	3.42	2.20	2.10	1.82	1.96	1.91	2.22	1.50	5.20	2.82	6.08
Total	99.26	99.20	99.06	99.50	98.80	99.69	99.33	98.72	98.84	99.18	98.97
						ppm					
Cs	0.9	0.2	2.6	0.5	1.1	0.30	0.23	0.2	0.3	0.2	0.4
Rb	2.2	14	74	33	42	29	10	14	63	52	37
Sr	191	328	399	565	790	636	479	745	169	829	681
Ba	325	534	484	473	559	972	331	464	603	643	678
Sc	29.22	28.09	29.54	21.25	23.21	23.60	26.80	19.01	31.81	21.71	28.96
V	253	288	281	294	306	402	465	234	267	259	250
Cr	1200	114	57	25	332	4	102	48	777	192	690
Co	60	46	49	37	37	45	44	26	46	35	36
Ni	454	65	52	26	111	25	70	13	186	88	140
Y	16.63	20.33	22.34	35.77	32.33	41.30	35.80	31.53	21.07	20.78	18.31
Zr	74	92	117	310	273	361	281	317	171	202	156
Hf	2.2	2.2	3.0	7.1	6.0	8.7	7.1	7.5	4.5	5.0	4.0
Nb	11	16	10	46	45	47	32	52	33	39	30
Ta	0.8	2.0	0.9	3.0	2.9	3.3	2.1	3.3	2.3	2.7	2.1
U	0.3	0.3	0.9	1.6	1.2	1.6	1.6	2.3	0.7	1.2	0.8
Th	0.9	1.2	3.2	7.7	5.6	6.9	3.5	12	3.2	3.8	3.0
Pb	5.6	11	17	113	40	6.5	4.2	20	5.6	8.3	7.8
						ppm					
La	10.05	12.43	19.14	56.75	49.14	53.4	323.0	69.20	32.75	34.04	27.07
Ce	18.52	24.57	40.61	103.9	87.30	115	72.9	123.8	57.14	62.89	51.74
Pr	2.36	3.07	4.63	12.59	10.83	14.8	10.0	14.73	7.33	7.45	6.23
Nd	10.71	13.90	19.42	49.78	43.24	60.3	43.1	54.06	28.99	29.14	24.68
Sm	2.96	4.07	5.16	11.32	10.12	11.1	8.55	11.32	6.56	6.52	5.76
Eu	1.06	1.44	1.58	3.31	3.05	3.47	2.90	3.01	1.97	1.94	1.74
Gd	3.76	4.68	5.05	9.31	9.21	9.92	7.76	8.57	5.45	5.32	5.27
Tb	0.61	0.66	0.84	1.42	1.25	1.52	1.28	1.31	0.78	0.80	0.70
Dy	3.43	4.07	4.52	7.76	7.06	8.37	7.09	6.79	4.55	4.51	3.98
Ho	0.68	0.85	0.91	1.53	1.40	1.52	1.33	1.35	0.92	0.90	0.76
Er	1.74	2.39	2.37	3.87	3.47	3.62	7.50	3.46	2.44	2.36	2.09
Tm	0.24	0.32	0.33	0.51	0.45	0.49	0.40	0.45	0.32	0.30	0.29
Yb	1.48	1.84	2.04	2.87	2.51	3.34	2.56	2.73	1.71	1.77	1.50
Lu	0.21	0.22	0.32	0.37	0.34	0.45	0.35	0.37		0.27	0.24

[1]P = picrite; Picb = picrobasalt; B = basalt; Bs = basanite; Tph = tephrite; Pr = peridotite.
Sources: EM-42, -37, -84, and -52 are from Xu et al., 2001; EM-70 and -83 are from Chung and Jahn, 1995; DD-11, and -17 and BZ-9 and -26 are from Zhang and Wang, 2002; others are from this study.

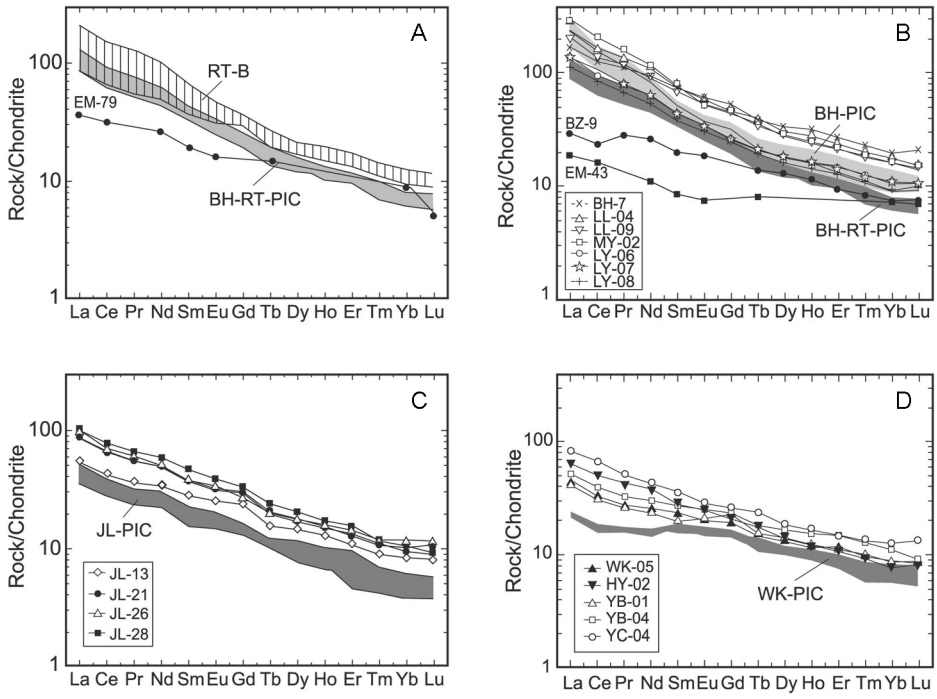

FIG. 3. Chondrite-normalized REE patterns of picrities and basalts in the ELIP. A. REE patterns of the middle-level picrite (EM-79) and other picrites (BH-RT-PIC, 5 samples) and associated basalts (RT-B, 7 samples) from Ertan (and Binchuan). B. REE patterns of the upper picrites (EM-43) (Xu et al., 2001) and associated basalt (BZ-9) (Zhang and Wang, 2002), and middle-level lavas (BH-PIC-B, BH-10, BH-11, BH-8), and low-level lavas (BH-RT-PIC) from Binchuan. Basalts from other districts are compared with the Binchuan lavas. C. REE patterns of the Lijiang picrites (JL-PIC, 8 samples) and intercalated basalts. D. REE patterns of low-La (WK-PIC) and high-La (WK-05) picritic rocks from Wulongba and picritic-basaltic rocks from Hanyi (HY-02) and Bailinshan districts (YB-01,Yb-04).

Bailinshan (La = 10.1 ppm) with comparable Yb abundance (Fig. 3D). Both the more evolved basaltic lavas from Yongsheng and Miyi exhibit similar LREE enrichment patterns with $(La/Yb)_N$ values of 13.4–17.1. Basalts from Bailinshan (YB-04) and Bingchuan (YC-04) show identical REE patterns to the Binchuan lavas (BH-PIC-B) (Fig. 3B), which are thought to be differentiated from picritic parental magma. Alkaline basalts from Yongning have an LREE enrichment pattern with $(La/Yb)_N$ of 12.2–13.0, identical to that of the basalts associated with picritic lavas and the overlying trachytic-rhyolitic succession at Ertan.

Trace elements

As large-ion lithophile elements (LILE: Rb, Ba, Sr) and Pb are easily affected by the post-magmatic alteration, altered samples obviously deviate from LILE-Nb positive correlation trends (Yang et al. (1998). Thus, samples deviating from the trend are filtered out, before describing the characteristics of incompatible elements for the picrites and basalts in the ELIP. The least altered rocks display variable abundances and ratios of incompatible elements (Table 1), and exhibit diverse primitive mantle–normalized abundance patterns (NAP) of trace elements (Fig. 4).

At Ertan, picrites show weak negative Nb anomalies and strong negative P anomalies as seen in the NAP diagram (Fig. 4A), and variable Ba/Nb (11–42), Th/Nb (0.08–0.16), and $(Ce/Yb)_N$ (3.6–23.0) ratios. A decreasing trend in Ba/Nb, Th/Nb, La/Nb, and $(Ce/Yb)_N$ is observed from basal picritic flow upward. Associated basalts display similar NAP as the picrites, suggesting crystal fractionation (Chung and Jahn, 1995). At Binchuan, most picrites display similar NAP as the Ertan picrites, but no obvious Nb anomalies (Fig. 4B), except for samples BH-8, 10, and 11 (BH-PIC-B), which are enriched in LREE and Th, but show obvious negative anomalies for the

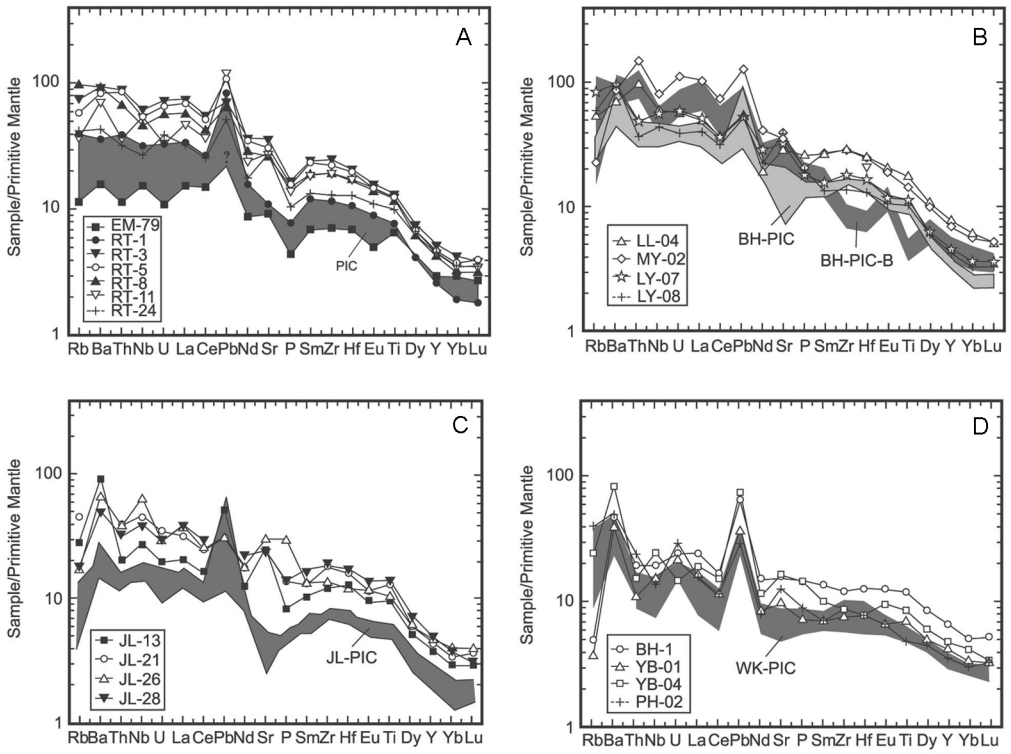

FIG. 4. Primitive mantle–normalized incompatible-element patterns (NAP) of the picrities and basalts in the ELIP. A. NAP of the picrites (EM-79, RT-1) and associated basalts from Ertan. B. NAP of the middle-level picrite and basalt (BH-PIC-B, BH-10, BH-11, BH-8) and other picrites (BH-PIC) from Binchuan. Basalts from other districts are compared with Binchuan lavas. C. NAP of the picrites (JL-PIC) and associated basalts from Lijiang. D. NAP of the picritic rocks from Wulongba (WK-PIC), Hanyi (HY-02), and Puhe (PH-02) and Bailinshan (YB-01, -04). Data of the primitive mantle from Sun and McDonough (1989).

high-field-strength elements (HFSE: Nb, Ta, Zr, Hf, Ti) (Fig. 4B). Most picrites from Binchuan have relatively low but variable Ba/Nb (2–26), Th/Nb (0.06–0.14), La/Nb (0.6–1.6), $(Ce/Yb)_N$ (2.2–10.0), and Nb/U (28–38) ratios, but samples BH-8, 10, and 11 yielded obviously high Th/Nb (0.17–0.23), La/Nb (1.25–1.40), and low Nb/U (20–24) ratios. The Lijiang picrites display a limited variation in abundances and ratios of incompatible elements, like REE (Table 1). Their NAP is similar to that of picrites from Ertan and Binchuan, but show relatively low abundances of incompatible elements (Fig. 4C). These picrites show weak positive Nb anomalies or are without anomalies, but exhibit obvious negative Sr anomalies, whereas the associated basalts show positive Nb anomalies and weak negative P anomalies (Fig. 4C). The picritic intrusives in the Dali (Wulongba, Puhe, and Hanyi) and picritic lavas from Bailinshan, although having low abundances of REE and HFSE (Fig. 4D), yield a wide range of Th/Nb (0.8– 0.2), Ba/Nb (24– 38), and a limited variation in La/Nb (0.8–1.2) and $(Ce/Yb)_N$ (2– 6) ratios. The alkaline basalts (LY-07 and -08) from Yongning lack HFSE anomalies, whereas basalt (LL-04) from Yongsheng resembles the Yongning basalts in incompatible element characteristics (Fig. 4D). The basalt (MY-02) from Miyi, a very evolved lava with low MgO content of 3.46 wt%, is also rich in LREE and Th, and has a pronounced negative Nb anomaly, but no negative anomalies of Zr, Hf, and Ti (Fig. 4D).

Sr, Nd and Pb isotopes

Nd and Sr isotopic compositions of the picritic-basaltic rocks in the ELIP are characterized by a wide $\varepsilon_{Nd(t)}$ range of 4.84 to –4.00 and $(^{87}Sr/^{86}Sr)_i$ of

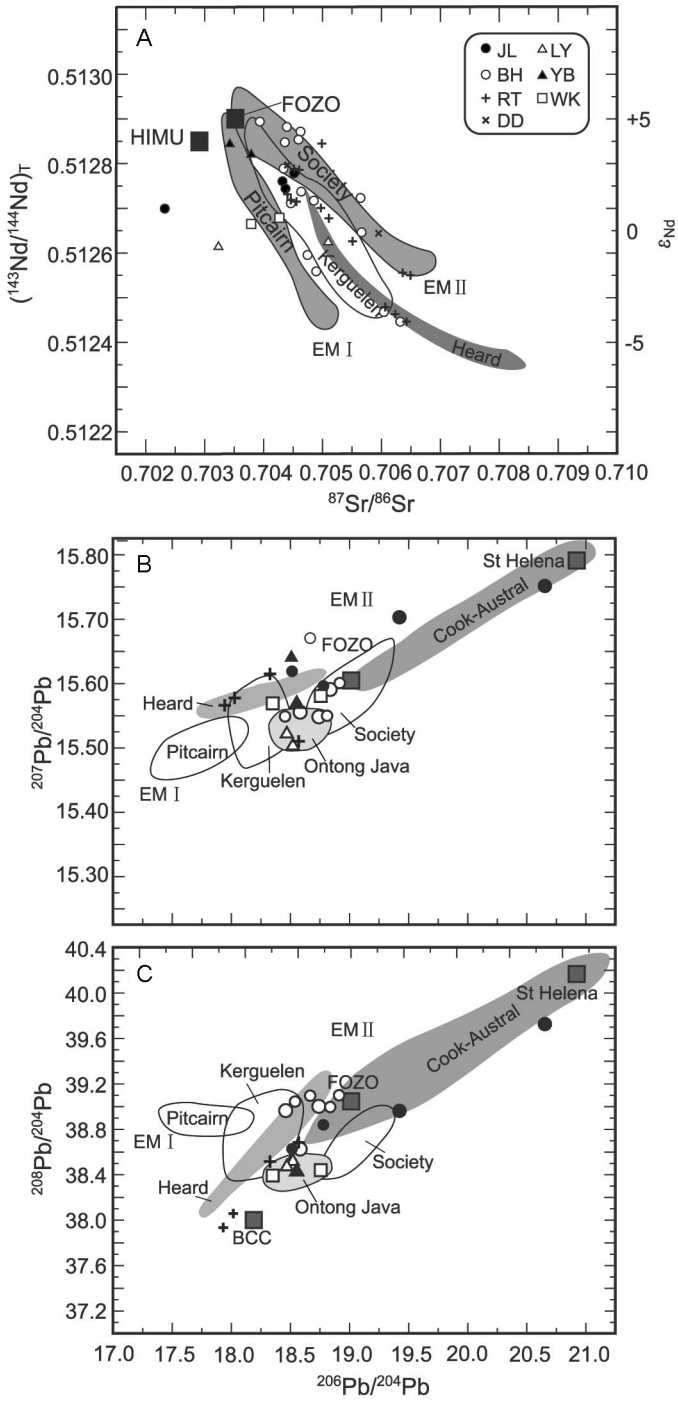

FIG. 5. *See caption on facing page.*

FIG. 5. Variation diagrams for Sr, Nd, and Pb isotopes of picrites and basalts from the ELIP. A. $(^{87}Sr/^{86}Sr)_i$ vs. $(^{143}Nd/^{144}Nd)_t$. B. $^{207}Pb/^{204}Pb$ vs. $^{206}Pb/^{204}Pb$. C. $^{208}Pb/^{204}Pb$ vs. $^{206}Pb/^{204}Pb$. Additional data in the area (Song et al., 2001b; Xu et al., 2001) were plotted in Figure 5A. Data sources as follows: End-members of mantle from Hofmann and White (1982), Zindler and Hart (1986), Hart (1988), and Hart et al. (1992); St Helena from Kogiso et al. (1997); Kerguelen from Gautier et al. (1990) and Weis et al. (1993); Heard from Barling et al. (1994); Society from White and Duncan (1996); Pitcairn from Woodhead and Devey (1993); Cook-Austral from Nakamura and Tatsumoto (1988); Ontong Java from Mahoney and Spencer (1991) and Mahoney et al. (1993). Abbreviations: PM = primitive mantle (McDonough and Sun, 1995); BCC = bulk continental crust (Rudnick and Fountain, 1995). Symbols are the same as in Figure 2, but a larger one for picrite, and a smaller one for basalt.

0.7023–0.7064 (Table 2; Fig. 5A). Most of Sr-Nd isotopic data fall in the field of worldwide OIBs (Wooden et al., 1993). Like REE and trace elements, three groups of picritic-basaltic rocks from Binchuan have been recognized (Fig. 5A). The uppermost picrite-basalts yielded a range of $\varepsilon_{Nd(t)}$ varying from 4.84 to 1.70 and $(^{87}Sr/^{86}Sr)_i$ of 0.7042–0.7056 (Table 2), and fall in the field of the Society Island lavas, showing an array between FOZO and EM II end-members (White and Duncan, 1996). The middle-level picrite and basalt yielded a limited range in $\varepsilon_{Nd(t)}$ of –1.10 to –1.75 and $(^{87}Sr/^{86}Sr)_i$ of 0.7047–0.7049 (Table 2), close to the array of Pitcairn Island basalts seen in Figure 5A. The lower-level picrites and underlying basalts yielded a range of $\varepsilon_{Nd(t)}$ varying from 1.32 to 1.16 and –3.58 to –4.07 and $(^{87}Sr/^{86}Sr)_i$ of 0.7044–0.7048, and 0.7063–0.7061, respectively (Table 2), and fall within the Heard Island array (Barling et al., 1994) (Fig. 5A).

The Sr-Nd isotopic signature of the Ertan lavas is similar to that of the Binchuan lavas; three groups also on appear Figure 5A. The first group includes the basal picrite and associated basalt, which have the lowest $\varepsilon_{Nd(t)}$ (–3.3 to –4.0) in the entire sequence, and lie on the Heard trend seen in Figure 5A. Their Sr-Nd isotopic signature is very similar to that of low-$\varepsilon_{Nd(t)}$ lavas from Binchuan (Fig. 5A). The second group, including other lavas in the Ertan section, yielded an array similar to that of the Society Island lavas (Fig. 5A). The third group includes picrites collected from different levels of a 50 m thick flow (Chung and Jahn, 1995), and yielded intermediate $\varepsilon_{Nd(t)}$ (1.4–1.7) and $(^{87}Sr/^{86}Sr)_i$ (0.7044–0.7045), except for sample EM-58 collected from the highest level. They fall in the field of the Kerguelen Island lavas (Gautier et al., 1990; Weis et al., 1993) and form an array with lavas in the first group, paralleling the Heard trend (Fig. 5A).

Although the Lijiang lavas show limited variation in REE abundances and patterns, they yielded a much wider range of $(^{87}Sr/^{86}Sr)_i$, varying from 0.70229 to 0.7045 from the upper part of the volcanic sequence downward (Table 2). Most of these samples fall within the field of the Kerguelen Island lavas seen in Figure 5A, and only one sample (JL-29) is far away from the field. Picritic rocks from Wulongba and Bailinshan fall in the field of the Pitcairn Island basalts (Woodhead and Devey, 1993), but the latter is close to the FOZO end-member (Campbell, 1998) on the $\varepsilon_{Nd(t)}$-ε_{Sr} diagram (Fig. 5A).

Pb isotopes of the picrites and associated basalts in the ELIP are characterized by a wide range of $^{206}Pb/^{204}Pb$ (18.034–20.641), $^{207}Pb/^{204}Pb$ (15.525–15.749), and $^{208}Pb/^{204}Pb$ (37.945–39.715), forming arrays that are aligned subparallel to the Northern Hemisphere reference line (NHRL) and to the right of the geochron (Figs. 5B and 5C). Both ends of the arrays point toward St. Helena, HIMU basalts, and the Heard Island lavas with low $^{206}Pb/^{204}Pb$ ratios (17.75) (Barling et al., 1994), respectively. The former is represented by Lijiang sample JL-29 with the lowest $(^{87}Sr/^{86}Sr)_i$, and the latter by the Ertan lowest-level basalts with the lowest $\varepsilon_{Nd(t)}$ (Figs. 5B and 5C). The Binchuan basalts with the highest $\varepsilon_{Nd(t)}$ are the closest to the FOZO end-member, whereas rocks from Bailinshan, Wulongba, and Yongning are close to the Ontong Java lavas (Mahoney and Spencer, 1991; Mahoney et al., 1993) plotted on Figures 5B and 5C.

Figure 6 further demonstrates that most samples in the picrite-cluster field have intermediate Sr, Nd, and Pb isotopic compositions; a few samples lie toward the ends of the Sr-Nd-Pb isotopic arrays. The Lijiang lavas lie in the field of the Cook-Austral Island lavas shown on Figures 6B and 5C, thus showing isotopic affinity with them (Nakamura and Tatsumoto, 1988), whereas some lavas from Ertan

TABLE 2. Sr, Nd, and Pb Isotopic Data of Representative Picritic-Basaltic Rocks in the ELIP

Location	Section	Sample	Rock	$^{87}Sr/^{86}Sr$	$(^{87}Sr/^{86}Sr)_T$	$^{143}Nd/^{144}Nd$	ε_{Nd}	$^{206}Pb/^{204}Pb$	$^{207}Pb/^{204}Pb$	$^{208}Pb/^{204}Pb$
Lijiang	Upper	JL-29	Picrite	0.70484	0.70229	0.512590	0.93	20.641	15.749	39.715
		JL-26	Basalt	0.70456	0.70436	0.512621	1.88	18.793	15.593	38.833
	Lower	JL-13	Basalt	0.70489	0.70450	0.512687	2.49	18.525	15.617	38.626
		JL-3	Picrite	0.70467	0.70432	0.512653	2.15	19.430	15.700	38.964
Bichuan	Upper	EM-52[a]	Basalt	0.70455	0.70432	0.512742	3.90			
		EM-49[a]	Basalt	0.70452	0.70433	0.512663	2.81			
		EM-48[a]	Basalt	0.70457	0.70436	0.512768	4.57			
		EM-43[a]	Picrite	0.70538	0.70462	0.512660	1.70			
		EM-42[a]	Basalt	0.70418	0.70392	0.512779	4.84			
		BZ-9[b]	Basalt	0.70481	0.70461	0.512810	4.40	18.843	15.602	39.107
		BZ-19[b]	Basalt	0.70470	0.70556	0.512743	4.10	18.584	15.555	39.068
	Middle	BH-10	Picrite	0.70518	0.70488	0.512395	–1.75	18.745	15.548	39.014
		BH-11	Basalt	0.70508	0.70471	0.512426	–1.10	18.678	15.669	39.097
	Lower	BH-15	Picrite	0.70525	0.70441	0.512576	1.16	18.593	15.555	38.644
		BH-19	Picrite	0.70563	0.70484	0.512580	1.32	18.847	15.591	39.010
		BZ-26[b]	Basalt	0.70587	0.70567	0.512495	–0.10	18.436	15.550	38.931
		EM-37[a]	Basalt	0.70696	0.70632	0.512321	–4.07			
		EM-35[a]	Basalt	0.70671	0.70605	0.512332	–3.58			
Ertan	Upper	R-11	Basalt	0.70606	0.70549	0.512493	–0.36	18.335	15.614	38.540
		EM-84[a]	Basalt	0.70534	0.70492	0.512554	1.12			
		EM-83[c]	Picrite	0.70541	0.70458	0.512680	2.80			
	Middle	EM-78[a]	Basalt	0.70561	0.70506	0.512571	0.66			
		EM-79[c]	Picrite	0.70586	0.70492	0.512760	4.00			
	Lower	EM-72[a]	Basalt	0.70676	0.70630	0.512399	–2.06			
		EM-73[a]	Basalt	0.70722	0.70646	0.512387	–2.38			
		RT-5	Basalt	0.70747	0.70619	0.512310	–3.64	18.034	15.575	38.077
		RT-1	Picrite	0.70713	0.70602	0.512333	–3.25	17.960	15.565	37.945
		EM-70[c]	Picrite	0.70647	0.70638	0.512290	–4.00			
Panzhihua	Upper	EM-58[c]	Picrite	0.70488	0.70446	0.512670	2.80			
		EM-56[c]	Picrite	0.70501	0.70439	0.512610	1.70			
	Lower	EM-57[c]	Picrite	0.70480	0.70441	0.512590	1.50			
		EM-55[c]	Picrite	0.70497	0.70451	0.512600	1.40			
Bailinshan		YB-04	Basalt	0.70443	0.70373	0.512740	3.46	18.518	15.639	38.552
		YB-01	Picrite	0.70362	0.70340	0.512769	3.91	18.569	15.569	38.448
Wulongba		WK-05	Picrite	0.70535	0.70422	0.512593	0.59	18.365	15.566	38.392
		WK-10	Picrite	0.70551	0.70374	0.512633	0.32	18.766	15.578	38.452
Yongniang		LY-06	Basalt	0.70929	0.70320	0.512469	–0.69	18.529	15.508	38.552
		LY-07	Basalt	0.70605	0.70508	0.512475	–0.48	18.473	15.525	38.503
Yongsheng		DD-11[b]	Basalt	0.70545	0.70593	0.512510	–0.10	18.855	15.581	39.343
		DD-17[b]	Basalt	0.70467	0.70437	0.512686	2.90	18.732	15.528	38.928

Sources: This study, unless otherwise specified as: a = Xu et al., 2001; b = Zhang and Wang, 2002; c = Chung and Jahn, 1995.

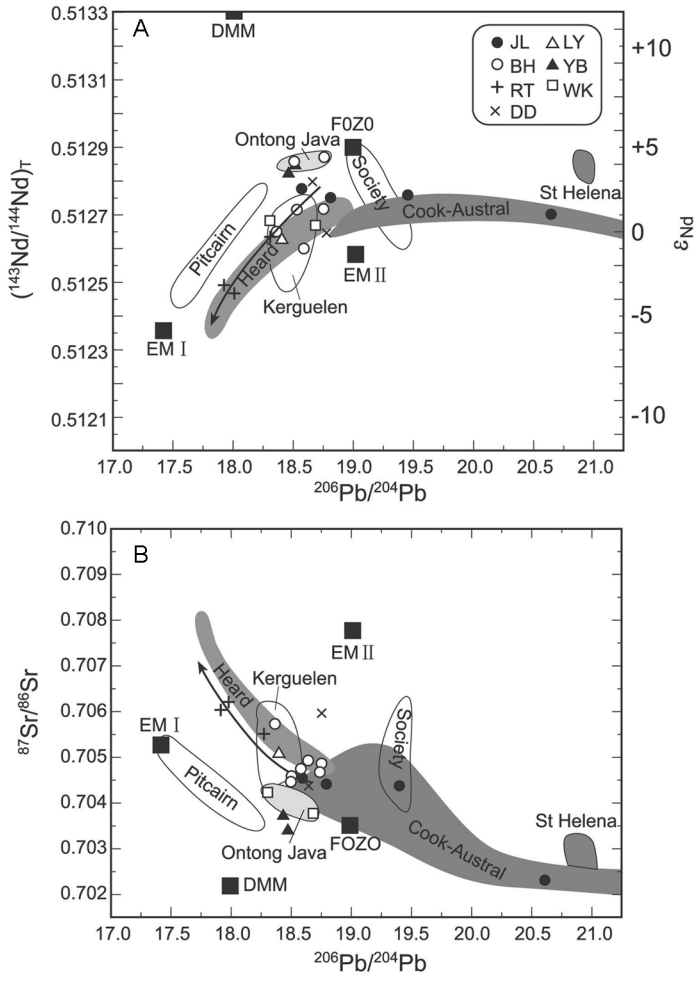

FIG. 6. Diagrams of $^{206}Pb/^{204}Pb$ vs. $(^{14}Nd/^{144}Nd)_t$ (A) and $^{206}Pb/^{204}Pb$ vs $(^{87}Sr/^{86}Sr)_I$ (B) for picrites and basalts from the ELIP. Additional data for basalts in the area (Song et al., 2001b) were plotted in the figures. Symbols are the same as in Figure 2, but a larger one for picrite, and a smaller one for basalt.

lie with the Heard Island lavas, and therefore are here called "Heard-like" lavas.

Discussion

The geochemistries of picrite and associated basalts in the ELIP are characterized by wide ranges of incompatible-element ratios (i.e., Th/Nb, La/Nb, Zr/Nb, Ba/Nb, La/Sm, Ce/Yb, etc.) and Sr-Nd-Pb isotopic compositions (Figs. 5–7). In Figure 7, they yielded two or three separated coherent trends, which intersect at an end-point with the lowest coherent ratios, close to the Ontong Java cluster (Mahoney and Spencer, 1991; Mahoney et al., 1993). As seen in Figures 5 and 6, they yield diverse arrays, or follow different covariation trends (i.e., Heard trend, Cook-Austral trend), and intersect at or near the FOZO or Ontong Java groupings with intermediate isotopic ratios. These geochemical characteristics indicate that the lavas were probably derived from the Emei plume axis, involving very complicated processes that led to heterogeneity of the source for generating the ELIP.

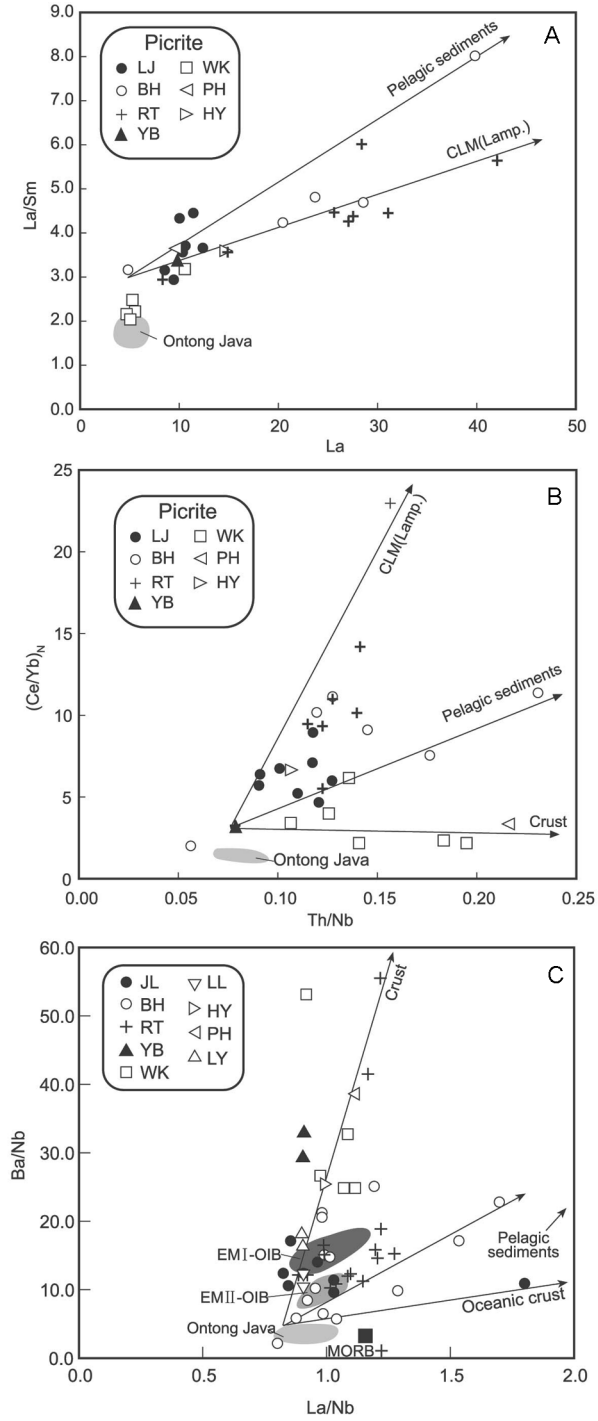

FIG. 7. Plots of La vs. La/Sm (A), $(Ce/Yb)_N$ vs. Th/Nb (B), and Ba/Nb vs. La/Nb (C) of the picrites and basalts from the ELIP. Data source: Ontong Java from Mahoney and Spencer (1991) and Mahoney et al. (1993), EM I-OIB and EM II-OIB from Weaver (1991). Additional data from for picrites and basalts in the area (Song et al., 2001b; Xu et al., 2001) were also plotted in the figures.

Geochemical end-member and possible source

Based on the above data, at least three lava groups exist: (1) the Ontong Java-like group with low $(^{87}Sr/^{86}Sr)_i$ (<0.7045) and high $\varepsilon_{Nd(t)}$ (>2.5); (2) the Cook-Austral–like group with high $^{206}Pb/^{204}Pb$ (>19.0) and low $(^{87}Sr/^{86}Sr)_i$ (<0.7045); (3) the Heard-like group with high $(^{87}Sr/^{86}Sr)_i$ (0.7044–0.7060), and low $\varepsilon_{Nd(t)}$ (1.7 to –3.0), $^{206}Pb/^{204}Pb$ (18.75–18.03), and $^{208}Pb/^{204}Pb$ (37.8–39.0). Coupled variations of Nd, Sr, and Pb isotopic compositions of these three groups can be interpreted as reflecting the mixing of identifiable mantle components (Zindler and Hart, 1986; Hart, 1988; Hart et al., 1992; Farley et al., 1992; Hanan and Graham, 1996), as well as processes involving crustal assimilation and plume-lithosphere interaction (Chung and Jahn, 1995).

Heard-like group

The Heard-like group includes lavas of the first and third groups of the Ertan volcanic sequence (Table 2) and the lower picrite-basalt flows (Table 2) of the Binchuan volcanic sequences (see Figs. 5A and 6). These lavas fall on the Heard trend, and show linear Pb-Pb (Figs. 5B and 5C) and curvilinear Pb-Nd (Fig. 6A) and Pb-Sr isotopic covariations (Fig. 6B), observed in samples from Heard Island (Barling et al., 1994). Both the linear and curvilinear arrays of isotopic compositions are compatible with two-component mixing in a mantle plume. As there is limited Pb isotopic analysis, the available data are not sufficient to place tight constraints on end-members for the two mixing components but, using the method of Barling et al. (1994), least-squares regressions of these data nevertheless provide constraints on minimum Nd and maximum Sr isotopic ratios of the depleted end-member, and the minimum $^{206}Pb/^{204}Pb$ ratio of the enriched end-member. Nd and Sr isotopic ratios relevant to the depleted end-member are estimated to be >1.7 and <0.7048, respectively, whereas the extrapolated end-member of both $\varepsilon_{Nd(t)}$ and $(^{87}Sr/^{86}Sr)_i$ is most likely close to the FOZO component (see Fig. 6). Based on a possible mixing curve, the enriched end-member is estimated to be <17.75 for maximum $^{206}Pb/^{204}Pb$, >0.706 for minimum $(^{87}Sr/^{86}Sr)_i$, and <–4.0 for maximum $\varepsilon_{Nd(t)}$ at 259 Ma.

There are two possibilities for the origin of the enriched end-member with high $(^{87}Sr/^{86}Sr)_i$, low-ε_{Nd}, and high Pb/Sr, Pb/Nd and Nd/Sr ratios: (1) from the upper continent crustal component that was recycled into and modified the periodotitic mantle (Barling et al., 1994); and (2) a melt from continental lithosphere mixed with picritic magmas from the plume (Chung and Jahn, 1995). For the continent crustal component, at least two ways can modify the chemistry of the studied Heard-like lavas—i.e., transport to a deep OIB source region by subduction (White and Duncan, 1996), or contamination during emplacement of mafic magmas. Both ways would result in a low Sr/Nd ratios and negative Nb anomalies of coherent lavas. However, the enriched end-member for Heard-like lavas is isotopically far away from continental crust (BCC or UCC) based on Pb-Sr and Pb-Nd isotopic covariation diagrams (Figs. 5 and 6). These lavas do not show obvious negative Nb anomalies (Fig. 4), and all fall outside the field of the Siberia Nd 1-2 layer, which is interpreted as typical of crustal assimilation (Lightfoot et al., 1990; Wooden et al., 1993), on Zr/Nb vs. La/Nb and Nb/U vs. Th/Nb plots (Fig. 8). They yielded a trend separated from the Wulongba picritic rocks, possibly related to crustal assimilation (see below, Figs. 7 and 9B). Therefore, these lines of evidence do not support the assimilation of continental crust for the enriched end-member. Based on geochemistry of the incompatible elements and Sr-Nd isotope of the Heard-like lavas, the enriched end-member should have high $(Ce/Yb)_N$ (>50), Th/Nb (>0.15), La/Nb (>1.2) and low Sr/Nd ratios, as well as medium Nb depletion, high $^{87}Sr/^{86}Sr$, and low $^{143}Nd/^{144}Nd$ ratios (see Figs. 5–8). Olivine lamproites, regarded as a melt derived from continental lithospheric mantle (Nelson et al., 1986; Jaques et al., 1989), probably are ideal candidates for the enriched end-member. This suggestion is supported by following two observations: (1) lamproitic rocks usually have high Mg#, low heavy REEs and Y, a strong negative Sr anomaly, and a mild Nb-Ta anomaly (Nelson et al., 1986; Jaques et al., 1989), which are also characteristics of picritic samples in the ELIP; and (2) primitive mantle normalized trace element patterns of lamporitic rocks (Nelson et al., 1986) are broadly similar to those of the Heard-like picrites and associated basalts (Fig. 4). Thus, Heard-like lavas are interpreted here as formed by mixing of picritic melt derived from the Emei plume and small-volume lamproitic melt derived from the CLM in various proportions.

Cook-Austral–like group

Representative samples in this group are picrites (JL-3 and JL-29) from the Lijiang volcanic sequence, which yielded very high $^{206}Pb/^{204}Pb$ (19.43–20.64) and $^{207}Pb/^{204}Pb$ ratios (15.70–

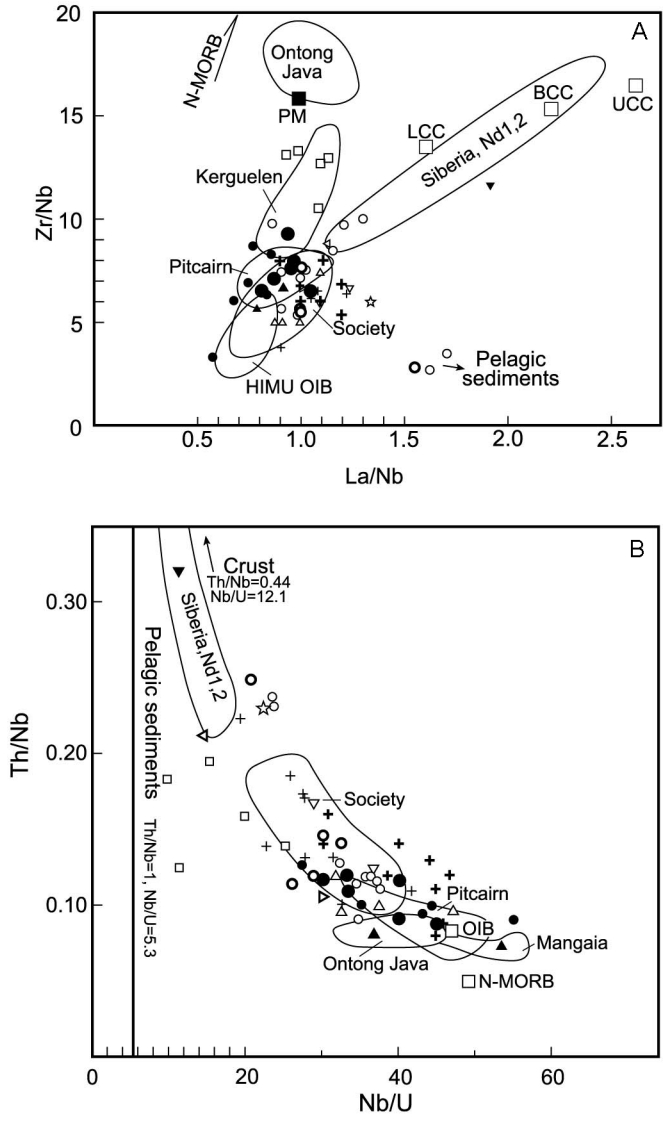

FIG. 8. Plots of Zr/Nb vs La/Nb (A) and Th/Nb vs Nb/U (B) for picrites and basalts from the ELIP. Additional data for picrites and basalts in the area (Song et al., 2001b; Xu et al., 2001) are also plotted. Data source: HIMU OIB from Weaver (1991) and Kogiso et al. (1997); Ontong Java from Mahoney and Spencer (1991) and Mahoney et al. (1993); Society from White and Duncan (1996); Pitcairn from Woodhead and Devey (1993); Kerguelen from Gautier et al. (1990). Siberia, Nd1, 2 corresponds to middle-lower Nadezhdinsky suite basalts of the Siberian Traps, Noril'sk area, and represent crustal contamination lavas (Lightfoot et al., 1990; Wooden et al., 1993). Abbreviations: PM = primitive mantle from McDonough and Sun (1995). CC and UCC: average compositions of bulk and upper continental crust respectively (Rudnick and Fountain, 1995; Barth et al., 2000). Pelagic sediments have Th/Nb of 1.0 and Nb/U of 5.3 (Woodhead, 1996). Symbols are the same as those in Figure 2.

15.75), but a wider range of $(^{87}Sr/^{86}Sr)_i$ (0.7023–0.7043) and lower ε_{Nd} (0.93–2.15) than MORB (Fig. 5A). Picrites and associated basalts from the Lijiang fall in the field of Cook-Austral island lavas (Nakamura and Tatsumoto, 1988), and show semi-linear Pb-Pb (Figs. 5A and 5B) and curvilinear Pb-Nd

(Fig. 6A) and Pb-Sr isotopic covariations (Fig. 6B), which also imply two-component mixing in a mantle plume.

Cook-Austral basalts with $^{206}Pb/^{204}Pb$ >20.5 are regarded as typical HIMU basalts (Nakamura and Tatsumoto, 1988). Similar rocks also occur in St. Helena in the southern Atlantic Ocean and in southern Polynesia, South Pacific (Chauvel et al., 1992; Kogiso et al., 1997). Such HIMU basalts are rare within continental flood basalts (Carlson, 1991); nevertheless, they were recently identified in African continental flood basalt (Stewart and Rogers, 1996; Franz et al., 1999; Rogers et al., 2000). This HIMU source is widely accepted as reflecting the involvement of subducted oceanic crust recycling into the deep mantle (Hofmann, 1982; Weaver, 1991; Chauvel et al., 1992; Kogiso et al., 1997).

Sample JL-29 has extremely high $^{206}Pb/^{204}Pb$ of 20.64 and extremely low $(^{87}Sr/^{86}Sr)_i$ of 0.7023, very similar to those of the most typical HIMU basalts from the Cook-Austral Islands (Fig. 6). Such high $^{206}Pb/^{204}Pb$ ratios can be produced by the involvement of subducted oceanic crust, because U/Pb and Th/Pb ratios of the oceanic crust increase during dehydration in the subduction zone, as demonstrated by experiments (Brenan et al., 1995; Kogiso et al., 1998). Much lower values of $(^{87}Sr/^{86}Sr)_i$ can be interpreted as derived from mixing of subducted oceanic crust with less-depleted mantle (Brenan et al., 1995). Moreover, JL-29 has lower contents of K_2O and P_2O_5 and lower abundances of incompatible elements (except for Nb) than other picrites in the ELIP, implying that its source is less enriched in incompatible elements relative to other sources, such as EM I and EM II that involved pelagic and continental sediments, respectively (Zindler and Hart, 1986). This source probably did not involve sediments, as smaller amounts of sediment would result in a source with high abundances of highly incompatible elements (Zr, Rb, Th, Nb, Ta, K, P, etc.). In contrast, although lower-level picrite (JL-3) and associated basalts (JL-13, JL-26) lie in the field of the Cook-Austral lavas, they yielded notably low $^{206}Pb/^{204}Pb$ (<18.80) and high $(^{87}Sr/^{86}Sr)_i$ (0.7044–0.7045) (Fig. 5). This departure from JL-29 suggests a component with relatively high $^{87}Sr/^{86}Sr$ and low $^{206}Pb/^{204}Pb$ mixing with the HIMU component in a plume. These lavas fall in the fields both of the Society and Kerguelen lavas seen in Figures 5, 6, and 8, also implying that this component probably results from a lesser amount of sediment interacting with depleted mantle (Weis et al., 1993; White and Duncan, 1996).

Ontong Java–like group

The Ontong Java–like group from all volcanic sequences in the ELIP includes picrites and associated basalts with low-La (< 10 ppm), low La/Sm (< 3.5), $(Ce/Yb)_N$ (< 5), Th/Nb(< 0.1), La/Nb(< 1.0), Zr/Nb (< 20), and Ba/Nb (< 10), (Figs. 7 and 8). They have high ε_{Nd} (> 3.0) and low $(^{87}Sr/^{86}Sr)_i$ (< 0.705), similar to the Sr-Nd isotopic signature of the FOZO component seen on Figure 5A, and intermediate $^{206}Pb/^{204}Pb$ (18.25–18.75), $^{207}Pb/^{204}Pb$ (15.50–15.60), and $^{208}Pb/^{204}Pb$ ratios (38.3–38.7), close to those of the Ontong Java lavas (Mahoney and Spencer, 1991; Mahoney et al., 1993) shown on Figures 5A and 5B. Representative samples that are the closest to the Ontong Java lavas include basalt (BZ-9, Zhang and Wang, 2002; 2003a, 2003b) and picrite (EM-43) at Binchuan (Xu et al., 2001), picrite (EM-79) at Ertan (Chung and Jahn, 1995), and picritic basalt (YB-01) at Bailinshan (Tables 1–2). These samples yielded a range of Th/Nb (0.06–0.09), La/Nb (0.7–1.1) and Nb/U (35–45) similar to Ontong Java analogues (Figs. 7 and 8). However, they yielded higher La/Sm (2.5–3.5), $(Ce/Yb)_N$ (2–4), and lower Zr/Nb (6–10) than those of Ontong Java (Figs. 7 and 8). This systematic departure can probably be attributed to processes of crystal fractionation or partial melting, which cause the variation in La/Sm, Ce/Yb, and Zr/Nb (White and Duncan, 1996). These samples fall in the field of the Ontong Java lavas on Pb-Pb isotopic covariation diagrams (Figs. 5A and 5B), which also suggests geochemical affinity with Ontong Java lavas.

The incompatible element ratios (Zr/Nb: 17.7; La/Nb: 1.0; Th/Nb: 0.08) of the Ontong Java lavas with high degrees of melting of 20–30% (Neal et al., 1997) indicate that its source is a little more depleted geochemically than primitive mantle. In the Pb-Sr and Pb-Nd isotopic plots (Fig. 6), both relatively depleted end-members for the Ontong Java and Society Island lavas point toward an average FOZO component, which led Campbell (1998) and White and Duncan (1996) to consider them as a FOZO component, a lower mantle material entrained by plume activity. In the ELIP, the more depleted picrites and associated basalts in the Ontong Java-like lavas also may be attributed to a large contribution of the FOZO component. In other words, these samples were probably derived from a high-degree of melting of lower-mantle material

entrained by the Emei plume, which is supported by the following three lines of evidence. First, all studied samples were collected from the axial zone of the Emei plume, marked by a the picrite-cluster field. The picritic magmas were probably derived from partial melting of the plume head or underlying the plume tail (Richard et al., 1989). High liquidus temperature > 1500ºC (Zhang and Wang, 2003a) and high degree of partial melting (> 20%) for these lavas require abnormal amounts of thermal energy, which is only provided by a plume head or tail from the lower mantle. Second, although different volcanic flows in the ELIP yielded two or three separately evolved trends for incompatible element covariations, the diverse trends intersect at an end-point with the lowest Th/Nb, La/Nb, Ba/Nb, La/Sm, and Ce/Yb ratios (see Fig. 7), suggesting a shared component in their source for the studied samples. The compositions of this end-point correspond to lavas of the Ontong Java group seen in Figure 7, indicating that this shared component should approach the FOZO component in the plume. Third, both end-members, estimated for the Heard-like and Cook-Austral–like lavas, overlap in a narrow area of Pb-Sr-Nd isotopic compositions, with the most depleted samples in the Ontong Java–like lavas (see Fig. 6), suggesting a significant role for a common component or a FOZO component for source mixing processes in the generation of the picrite and associated basalt within this overlapping area.

Terrigenous and pelagic sediments in the source

Besides the Heard-like lavas, most lavas from Binchuan and Ertan yielded an array like the Society Island lavas seen in the Sr-Nd isotopic diagram (Fig. 5A), in which a few samples tend toward the EMII end-member (Fig. 5A). Middle-level lavas (BH-10, BH-11) from Binchuan and two picritic rocks at Wulongba fall in or near the Pitcairn field and trend toward the EM I end-member (Fig. 5A). Many authors proposed that EM II and EM I sources involve recycling terrigenous and pelagic sediments by subduction (White and Hofmann, 1982; Weaver, 1991; Chauvel et al., 1992). Modeling calculations also demonstrated that mixing of depleted mantle with oceanic crust plus 5% terrigenous sediments in the source can explain the Sr-Nd isotopic variation of lavas like the Society group (EM II source), whereas mixing of depleted mantle with oceanic crust plus 5% pelagic sediments might explain the Sr-Nd isotopic covariation of lavas like Pitcairn (EM I source) (Chauvel et al., 1992). Therefore, the Society-like Sr-Nd isotopic arrays for some lavas from Binchuan and Ertan suggest involvement of subducted terrigenous sediments with oceanic crust. In contrast, Sr-Nd isotopic covariation of samples BH-10 and BH-11 probably reflects contribution of pelagic sediments in the magma source. This suggestion is supported by the incompatible-element study.

Although incompatible-element geochemistry of the pelagic sediments is less easily characterized, in part because abundances of some elements are highly variable in these sediments, and in part because geochemical processes in a subduction zone changes the compositions of these sediments (Irifune et al., 1994; Plank and Langmuir, 1998), some ratios, i.e., Pb/Ce, Nb/U, La/Nb, Th/Nb (and in some cases Ba/Nb), are valuable for qualitative demonstration of these deeply recycled sediments in the source (White and Duncan, 1996). Samples BH-10, BH-11, and BH-8 yielded a separate trend from other samples, and extend toward pelagic sediments with much higher La/Nb (3.3), Th/Nb (1.0), and Ba/Nb ratios (88.9) seen in Figure 7. These three samples obviously depart from other samples falling in the field of the Society and Pitcairn islands (Fig. 8B), and extend toward the pelagic sediments with high Th/Nb (1.0) and low Nb/U (5.3) ratios (Woodhead, 1996), as shown in Figure 9. Moreover, these samples have high La abundance (up to 40 ppm), relatively high La/Sm (Fig. 7A), and $(Ce/Yb)_N$ (Fig. 7B), but a low Zr/Nb ratio (Fig. 8A). As LREEs enter more easily into fluid during dehydration processes in a subduction zone, lavas involving a pelagic sediment component would thus yield high LREE abundance and high La/Sm and Ce/Yb ratios. Although La/Sm and Ce/Yb ratios, like the Zr/Nb ratio, are easily affected by magmatic processes (White and Duncan, 1996), they still reflect the contribution of a lesser amount of pelagic sediment component in the generation of these lavas.

Recycling of subducted materials

As mentioned above, trace elements and Sr-Nd-Pb isotopic systematics of the Lijiang picrites suggest a HIMU component in the source; some lavas from Binchuan and Ertan also record terrigenous and pelagic sediment components involved in generating these magmas. This HIMU component is most likely subducted oceanic crust, whereas terrigenous and pelagic sediments associated with oceanic crust probably was recycled into the deep mantle by subduction. If the oceanic crust was

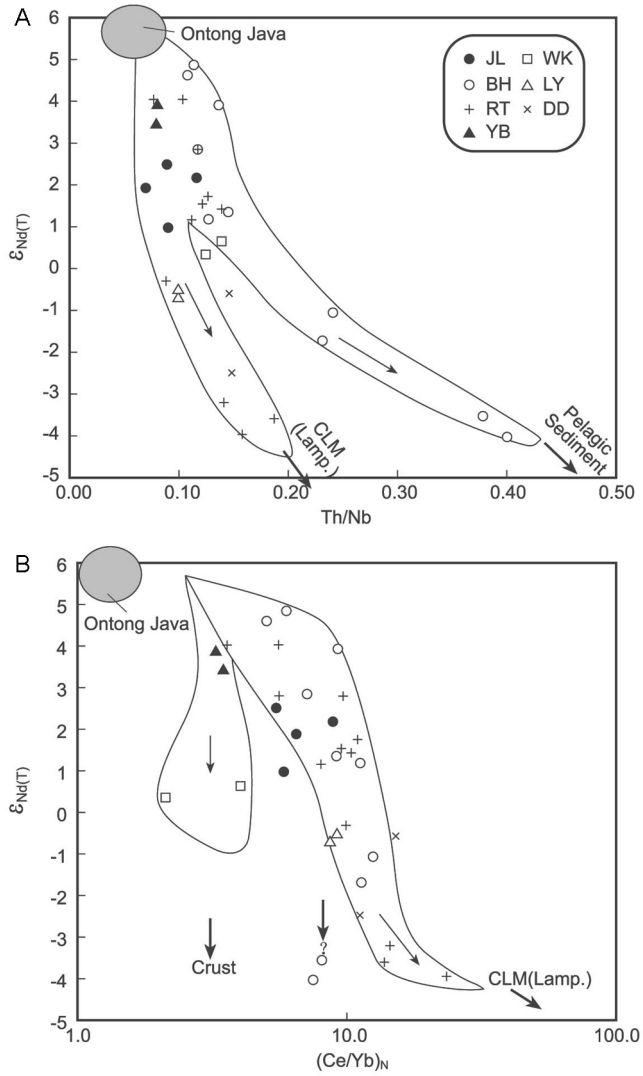

FIG. 9 Covariations of between $\varepsilon_{d(t)}$ and Th/Nb (A) and $(Ce/Yb)_N$ (B) for picrites and basalts from the ELIP. Data source: Ontong Java from Mahoney and Spencer (1991) and Mahoney et al. (1993). Lamproites and crust from Chung and Jahn (1995). The pelagic sediments have ε_{Nd} of < –5 and a Th/Nb ratio of 1.0 (White and Duncan, 1996). See text for explanation.

transported into the deep mantle, this recycling material must have transformed into eclogite. The appearance of the eclogite in the Emei plume may be constrained by incompatible elements in the lavas. Because heavy REE and Y are highly compatible in garnet, coherent ratios, e.g., Sm/Yb, Nb/Y, and Zr/Y, would increase with the increase of residual garnet in the garnet stability field during partial melting. If these ratios in the primary magma exceed the corresponding critical ratios of the low-degree melts of garnet-lherzolite, they can possibly prove the presence of an eclogite phase in the mantle plume. There are 13 samples with Sm/Yb ratios ranging from 4.02 to 6.3 (Fig. 10A), being much higher than those of Siberian, Deccan, and Columbia River basalts (< 3) (Lassiter and DePaolo, 1997). In Figure 10B, their Zr/Y ratios are intermediate between 4.5 and 13; Nb/Y ratios vary between 0.4

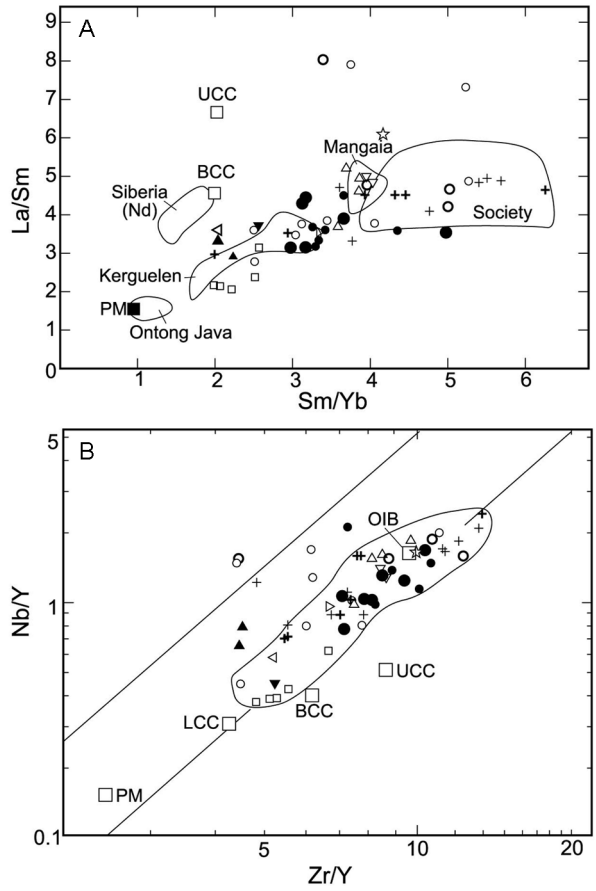

FIG. 10. Plots of La/Sm vs. Sm/Yb (A) and Nb/Y vs. Zr/Y (B) for picrites and basalts from the ELIP. In the lower panel, the parallel lines mark the upper and lower boundaries of the Iceland basalt data (Fitton et al., 1997). Other symbols and data sources are the same as in Figure 8.

and 2.1. The covariation of the ratios is similar to that of Kerguelen basalt (Frey et al., 2000). It is notable that the measured Nb/Y and Zr/Y ratios of these lavas are much higher than the calculated values of melts formed by low-degree melting of garnet-lherzolite. For example, when non-modal fractional melting of garnet-lherzolite reaches 1%, the Zr/Y ratio of the melt is only 10 (Fitton et al., 1997). Similarly, the Sm/Yb ratio calculated by the batch melting equation is also relatively low (Lassiter and DePaolo, 1997). This indicates that partial melting of garnet-lherzolite alone will not produce magmas with high Sm/Yb, Zr/Y, and Nb/Y ratios, even if the degree of melting is very small. Actually, it is impossible for the degree of melting for a magma derived from the high-temperature region of the plume axis to be very small (Campbell, 1998). However, if the source region is composed of eclogite-bearing iherzolite, this kind of magma can be easily explained by melting of a source with subducted oceanic crust. This explanation is also consistent with high-pressure experimental results on materials of continental and oceanic crust (Cordery et al., 1997; Hirose et al., 1999; Ono et al., 2001).

Crustal contamination

Because emplacement of the picritic and basaltic flows in the ELIP occurred in a continental environment, continental crust should be considered as a potential contamination. We conclude that picritic rocks in the Dali region (i.e., Wulongba, Hanyi, and Puhe) probably were modified by such crustal

assimilation. Their Pb-Sr and Pb-Pb isotopic compositions are close to those of the Bailinshan lavas with isotopic signatures similar to Ontong Java lavas (Figs. 5B, 5C, and 6B), but ε_{Nd} values are clearly low, which implies that a decrease in ε_{Nd} value is probably not related to pelagic sediment assimilation, but rather to contamination by the continental crust (see Fig. 9B). The following three observations support this possibility. First, these rocks occur as small stocks or dikes, intruded into the shallow upper crust; such melt bodies are easily contaminated by continental crust. Second, an extremely high Ba/Nb ratio and relatively invariable La/Sm and $(Ce/Yb)_N$ ratios of these rocks result in an independent variable trend in La/Sm vs. La (Fig. 7A), $(Ce/Yb)_N$ vs. Th/Nb (Fig. 7B), and $(Ce/Yb)_N$ vs. ε_{Nd} (Fig. 9B) plots. Third, these rocks yielded low Sm/Yb (Fig. 10A), Nb/Y and Zr/Y ratios (Fig. 10B), as well as high Th/Nb and low Nb/U ratios (Fig. 8). The coherent variations in incompatible element ratios are consistent with the assimilation of continental crust (BCC) (see Figs. 8b and 9).

Conclusions: Spatial Heterogeneity of the Source

The geochemistry of the trace elements and Sr-Nd-Pb isotopes of the picrite and associated basalts in the ELIP can be explained by processes involving: (1) partial melting of a heterogeneous, eclogite-bearing source to produce picritic magmas; (2) mixing of a small-volume melt from the CLM with the picritic magmas; and (3) crustal assimilation during mafic magma ascent. The heterogeneity of the mantle source is related to recycling of subducted oceanic crust and associated sediments into the deep mantle. Three components in the heterogeneous source, i.e., FOZO-like mantle, recycled oceanic crust, and sediments, have been recognized based on the incompatible element ratios and Sr-Nd-Pb isotopic systematics. If this is correct, mixing processes of two or more components may be regarded as playing an important role in the generation of the Emeishan CFB. Even in a 5×10^4 km^2 area, mixing of different components resulted in a very heterogeneous source for the plume head. The FOZO-like component, a lower mantle material entrained by a plume, is a common component, whereas other components—i.e., oceanic crust, terrigenous and pelagic sediments—are heterogeneous in the source for picrite and associated basalt in the ELIP. For example, at Lijiang, the mixed component is mainly subducted oceanic crust without—or with a lesser amount of—terrigenous sediments in the source. In contrast, at Binchuan, the mixed component is dominated by subducted sediments, including both terrigenous and pelagic sediments, whereas at Ertan, terrigenous sediments became the dominant (or predominant) component in the source. No other component mixed with the FOZO-like component can be identified in the source for the Bailinshan picrites. Evidently, a trend exists for variation in these components, changing from predominantly oceanic crust through both crust and sediments into terrigenous sediments in the source from a WNW to ESE direction within the picrite-cluster field (Fig. 1B).

Acknowledgments

This study was supported by the Outstanding Youth Foundation (to Z. Q. Hou) of the National Science Foundation of China, National Basic Research Plan Project 973 (to Hou) from the Ministry of Science and Technology, and the Geology Professional Foundation from the Ministry of Land and Mineral Resources. The authors express deep thanks to Profs. Lin Jianying and Zhang Rushi for their help during field work, and are grateful to Miss Chen Weishi and Miss Zhang Qiling for their assistance in finishing the manuscript.

REFERENCES

Barling, J., Goldstein, S. L., and Nicholls, I. A., 1994, Geochemistry of Heard Island (southern Indian Ocean): Characterization of an enriched mantle component and implications for enrichment of the sub-Indian ocean mantle: Journal of Petrology, v. 35, p. 1017–1053.

Barth, M. G., McDonough, W. F., and Rudnick, R. L., 2000, Tracking the budget of Nb and Ta in the continental crust: Chemical Geology, v. 165, p.197–213.

Brenan, J. M., Shaw, H. F., Phinney, D. L. and Ryerson, R. J., 1995, Ruite-aqueous fluid partitioning of Nb, Ta, Hf, Zr, U and Th: Implications for high field strength element depletion in island-arc basalts: Earth and Planetary Science Letters, v.128, p. 327–339.

Campbell, I. H., 1998. The mantle's chemical structure: Insights from the melting products of mantle plumes, *in* Jackson, I. N. S., ed., The Earth's mantle: Composition, structure and evolution: Cambridge, UK, Cambridge University Press, p. 259–310.

Campbell, I. H., and Griffiths, R. W., 1990, Implications of mantle plume structure for the evolution of flood

basalts: Earth and Planetary Science Letters, v. 99, p. 79–93.

Carlson, R. W., 1984, Isotopic constraints on Columbia River flood basalt genesis and the nature of the subcontinental mantle: Geochimica et Cosmochimica Acta, v. 48, p. 2357–2372.

Carlson, R. W., 1991, Physical and chemical evidence on the cause and source characteristics of flood basalt volcanism: Australian Journal of Earth Science, v. 38, p. 525–544.

Chauvel, C., Hofmann, A. W., and Vidal, P., 1992, HIMU-EM: The French Polynesian connection: Earth and Planetary Science Letters, v. 110, p. 99–119.

Chung, S. L., and Jahn, B. M., 1995, Plume-lithosphere interaction in generation of the Emeishan flood basalts at the Permian-Triassic boundary: Geology, v. 23, p. 889–892.

Chung, S. L., Jahn, B. M., and Wu, G. Y., 1998, The Emeishan flood basalt in SW China: A mantle plume initiation model and its connection with continental break-up and mass extinction at the Permian–Triassic boundary, *in* M.F.J. Flower et al., eds., Mantle dynamics and plate interaction in East Asia: American Geophysical Union, Geodynamics series, v. 27, p. 47–58.

Coffin, M. F., and Eldholm, O., 1994, Large igneous provinces: Crustal structure, dimensions, and external consequences: Reviews in Geophysics, v. 32, p. 1–36.

Cordery, M. J., Davies, G. F., and Campbell, I. H., 1997, Genesis of flood basalts from eclogite-bearing mantle plumes: Journal of Geophysical Research, v. 102, p. 20,179–20,197.

Courtillot, V., Jaupart, C., Manighetti, I., Tapponnier, P. and Besse, I., 1999, On causal links between flood basalts and continental breakup: Earth and Planetary Science Letters, v. 166, p. 177–195.

Farley, K. A., Natland, J. H., and Craig, H., 1992, Binary mixing of enriched and undegassed (primitive?) mantle components (He, Sr, Nd, Pb) in Samoan lavas: Earth and Planetary Science Letters, v. 111, p. 183–199.

Fitton, J. G., Saunders, A. D., Norry, M. J., Hardarson, B. S., and Taylor, R. N., 1997, Thermal and chemical structure of the Iceland plume: Earth and Planetary Science Letters, v. 153, p. 197–208.

Franz, G., Steiner, G., Volker, F., Pudlo, D., and Hammerschmidt, K., 1999, Plume related alkaline magmatism in central Africa—the Meidob Hills (W. Sudan): Chemical Geology, v. 157, p. 27–47.

Frey, F. A., Coffin, M. F., Wallace, P. J., Weis, D., and Zhao, X., 2000, Origin and evolution of a submarine large igneous province: the Kerguelen Plateau and Broken Ridge, southern Indian Ocean: Earth and Planetary Science Letters, v. 176, p. 73–89.

Gallagher, K., and Hawkesworth, C. J., 1992, Dehydration melting and the generation of continental flood basalts: Nature, v. 258, p. 57–59.

Gautier, I., Weis, D., Mennessier, J.-P., Vidal, P., Giret, A., and Loubet, M., 1990, Petrology and geochemistry of Kerguelen basalts (South Indian Ocean): Evidence of the mantle sources from ridge to an intraplate position: Earth and Planetary Science Letters, v. 100, p. 59–76.

Hanan, B. B., and Graham, D. W., 1996, Lead and helium isotope evidence from oceanic basalts for a common deep source of mantle plumes: Science, v. 272, p. 991–995.

Hart, S. R., 1988, Heterogeneous mantle domains: Signatures, genesis and mixing chronologies: Earth and Planetary Science Letters, v. 90, p. 273–296.

Hart, S. R., Hauri, E., Oschmann, L., and Whitehead, J., 1992, Mantle plumes and entrainment: Isotopic evidence: Science, v. 256, p. 517–520.

Hauri, E. H., and Hart, S. R., 1993, Re-Os systematics of HIMU and EM? oceanic island basalts from the south Pacific Ocean: Earth and Planetary Science Letters, v. 114, p. 353–371.

Hawkesworth, C. J., Mantovani, M., and Peate, D., 1988, Lithosphere remobilization during Parana CFB magmatism: Journal of Petrology, Special Lithosphere Issue, p. 205–223.

Hergt, J. M., Peate, D. W., and Hawkesworth, C. J., 1991. The petrogenesis of Mesozoic Gondwana low-Ti flood basalts: Earth and Planetary Science Letters, v. 105, p. 134–148.

Hirose, K., Fei, Y., Ma, Y., and Mao, H. K., 1999, The fate of subducted basaltic crust in the Earth's lower mantle: Nature, v. 397, p. 53–56.

Hofmann, A. W., 1997, Mantle geochemistry: The message from oceanic volcanism: Nature, v. 385, p. 219–229.

Hofmann, A. W., and White, W. M., 1982, Mantle plumes from ancient oceanic crust: Earth and Planetary Science Letters, v. 57, p. 421–436.

Hou, Z. Q., Lu, J. R., Wang, Y. L., Xia, L. Q., Li, H. Y., and Guo, L. J., 1999, The Emei igneous province: Characteristics and origin: Geological Review, v. 45, p. 885–891 (in Chinese with English abstract).

Irifune, T., Ringwood, A. E., and Hibberson, W. O., 1994, Subduction of continental crust and terrigenous and pelagic sediments: an experimental study: Earth and Planetary Science Letters, v. 126, p. 351–368.

Jaques, A., Sun, S. S., and Chappell, B. C., 1989, Geochemistry of the Argyle (AK 1) lamproite pipe, Western Australia, *in* Ross, J. et al., eds., Kimberlites and related rocks: Geological Society of Australia, Spec, Publ., v. 14, p. 170–188.

Kogiso, T., Hirose, K., and Takahashi, E., 1998, Melting experiments on homogeneous mixtures of peridotite and basalt: Application to the genesis of oceanic island basalts: Earth and Planetary Science Letters, v. 162, p. 45–61.

Kogiso, T., Tatsumi, Y., Shimoda, G., and Barsczus, H. G., 1997, High μ (HIMU) ocean island basalts in southern Polynesia: New evidence for whole mantle scale recy-

cling of subducted oceanic crust: Journal of Geophysical Research, v. 102, p. 8085–8103.

Lassiter, J. C., and Depaolo, D. J., 1997, Plume/lithosphere interaction in the generation of continental and oceanic flood basalts: Chemical and Isotopic Constraints, *in* Mahoney, J. J., and Coffin, M. F., eds., Large igneous provinces: Continental, oceanic, and planetary flood volcanism: American Geophysical Union, Geophysical Monograph no. 100, p. 335–356.

Lightfoot, P. C., Hawkesworth, C. J., Hergt, J., Naldrett, A. J., Gorbachev, N .S., Fedorenko, V. A., and Doherty, W., 1993, Remobilization of the continental lithosphere by a mantle plume: Major-, trace-, and Sr-, Nd-, and Pb-isotope evidence from picritic and tholeiitic lavas of the Noril'sk district, Siberian trap, Russia: Contributions to Mineralogy and Petrology, v. 114, p. 171–188.

Lightfoot, P. C ., Naldrett, A. J., Gorbachev, N. S., Doherty, W., Fedorenko, V. A., 1990, Geochemistry of the Siberian Trap of the Noril'sk area, USSR, with implications for the relative contributions of crust and mantle to flood basalt magmatism: Contributions to Mineralogy and Petrology, v. 104, p. 631–644.

Lin, J. Y., 1981, Study on the geology and petrochemistry of Permian basalts, Chenghai-Erhai district, Yunnan: Bulletin of Chengdu Institute of Geology and Mineral Resources, v. 2, p. 49–68 (in Chinese).

Lu, J. R., 1996, Dynamical characteristics of the Emei mantle plume: Acta Geoscientia Sinica, v.17, p. 424–438 (in Chinese).

Mahoney, J. J., and Spencer, K. J., 1991, Isotopic evidence for the origin of the Manihiki and Ontong Java plateaus: Earth and Planetary Science Letters, v. 104, p. 196–210.

Mahoney, J. J., Storey, M., Duncan, R. A., Spencer, K. J., and Pringle, M., 1993, Geochemistry and age of the Ontong Java plateau, *in* Pringle, M. S., et al., The Mesozoic Pacific: Geology, tectonics, and volcanism: American Geophysical Union, Geophysical Monograph 77, p. 233–261.

McDonough, W. F., and Sun, S. S., 1995, Composition of the Earth: Chemical Geology, v. 120, p. 223–253.

Menzies, M. A., 1992. The lower lithosphere as a major source for continental flood basalts: A re-appraisal, *in* Storey B. C. et al., eds., Magmatism and the causes of continental break-up: Geological Society of London, Special Publication, v. 68, p. 33–41.

Nakamura, Y., and Tatsumoto, M., 1988, Pb, Nd, Sr isotopic evidence for a multicomponent source for rocks of Cook-Austral Islands and heterogeneities of mantle plumes: Geochimica et Cosmochimica Acta, v. 52, p. 2909–2924.

Neal, C. R., Mahoney, J. J., Kroenke, L. W., Duncan, R. A., and Petterson, M. G., 1997, The Ontong Java Plateau, *in* Mahoney, J. J., and Coffion, M. F., eds. Large igneous provinces: Continental, oceanic, and planetary flood volcanism: American Geophysical Union, Geophysical Monograph, no. 100, p. 183–216.

Nelson, D. R., McCulloch, T. M., and Sun, S. S., 1986, The origin of ultrapotassic rocks as inferred from Sr, Nd and Pb isotopes: Geochimica et Cosmochimica Acta, v. 50, p. 231–245.

Ono, S., Ito, E., and Katsura, T., 2001, Mineralogy of subducted basaltic crust (MORB) from 25 to 37 Gpa, and chemical heterogeneity of the lower mantle: Earth and Planetary Science Letters, v. 190, p. 57–63.

Plank, T., and Langmuir, C. H., 1998, The chemical composition of subducting sediment and its consequences for the crust and mantle: Chemical Geology, v. 145, p. 325–394.

Reiberg, L., Zindler, A., Marcantonio, F., White, W., Wyman, D., and Weaver, B., 1993, Os isotope systematics in ocean island basalts: Earth and Planetary Science Letters, v. 120, p. 149–167.

Richard, M. A., Duncan, R. A., and Courtillot, V. E., 1989, Flood-basalt and hot spot tracks: Plume heads and tails: Science, v. 246, p. 103–107.

Rogers, N., Macdonald, R., Fitton, J. G., George, R., Smith, M., and Barreiro, B., 2000, Two mantle plumes beneath the East African rift system: Sr, Nd, and Pb isotope evidence from Kenya Rift basalts: Earth and Plantary Science Letters, v. 176, p. 387–400.

Rudnick R. L., and Fountain, D. M., 1995, Nature and compositon of the continental crust: A lower crustal perspective: Reviews in Geophysics, v. 33, p. 267–309.

Song, X. Y., Hou, Z. Q., Cao, Z. M., Lu, J. R., Wang, Y. L., Zhang, C. J., and Li, Y. G., 2001a, Geochemical characteristics and period of the Emei igneous province: Acta Geologica Sinica, v.75, p. 498–506 (in Chinese with English abstract).

Song, X. Y., Hou, Z. Q., Huang, Y. J., Zhang, C. J., and Wang, Y. L., 1999, REE indicator of mantle plume in Emei igneous province: Geological Review, v. 45, p. 872–875 (in Chinese with English abstract).

Song, X. Y., Zhou, M. F., Hou, Z. Q., Cao, Z. M., Wang, Y. L., and Li, Y. G., 2001b, Geochemical constraints on the mantle source of the upper Permian Emeishan continental flood basalts, southwestern China: International Geology Review, v. 43, p. 213–225.

Stewart, K., and Rogers, N., 1996, Mantle plume and lithosphere contributions to basalts from southern Ethiopia: Earth and Planetary Science Letters, v. 139, p. 195–211.

Sun, S. S., and McDonough, W. F., 1989, Chemical and isotopic systematics of oceanic basalts: Implications for mantle composition and processes, *in* Saunders, A. D., and Norry, M J., eds., Magmatism in the ocean basins: Geological Society of London, Special Publication, v. 42, p. 313–345.

Tatsumi, Y., 1986, Chemical characteristics of fluid phase released from a subduction lithosphere and origin of arc magma: Evidence from high-pressure experiments

and natural rocks: Journal of Volcanology and Geothermal Research, v. 29, p. 293–309.

Turner, S. P., and Hawkesworth, C . J., 1995, The nature of the subcontinental mantle: Constraints from the major element composition of continental flood basalts: Chemical Geology, v. 120, p. 295–314.

Weaver, B. L., 1991, The origin of ocean island basalt end-member compositions: Trace element and isotopic constraints: Earth and Planetary Science Letters, v. 104, p. 381–397.

Weis, D., Frey, F. A., Leyrit, H., and Gautier, I., 1993, Kerguelen Archipelago revisited: Geochemical and isotopic study of the southeast province lavas: Earth and Planetary Science Letters, v. 118, p. 101–119.

White, R. S. and McKenzie, D. P., 1995, Mantle plumes and flood basalts: Journal of Geophysical Research, v. 100, p. 17,543–17,585.

White, W. M., and Duncan, R. A., 1996, Geochemistry and geochronology of the Society Islands: New evidence for deep mantle recycling, *in* Basu, A., and Hart, S. R., eds., Earth processes: Reading the isotopic code: American Geophysical Union, Geophysical Monograph, no. 95, p. 183–206.

White, W. M. and Hofmann, A. W., 1982, Sr and Nd isotopie geochemistry of oceanic basalts and mantle evolution. Nature, v. 296, p.821–825.

Wooden, J. L., Czamanske, G. K., Fedorenko, V. A., Arndt, N. T., Chauvel, C., Bouse, R. M., King, B. S., Knight, R. J., and Siems, D. F., 1993, Isotopic and trace-element constraints on mantle and crustal contributions to Siberian continental flood basalts, Noril'sk area, Siberia: Geochimica et Cosmochimica Acta, v. 57, p. 3677–3704.

Woodhead, J. D., 1996, Extreme HIMU in an oceanic setting: the geochemistry of Mangaia Island (Polynesia), and temporal evolution of the Cook-Austral hotspot: Journal of Volcanology and Geothermal Research, v. 72, p. 1–19.

Woodhead, J. D. and Devey, C. W., 1993, Geochemistry of the Pitcairn seamounts, I: Source character and temporal trends: Earth and Planetary Science Letters, v. 116, p. 81–99.

Xu, Y. G., Chung, S. L., Jahn, B. M., and Wu, G. Y., 2001, Petrologic and geochemical constraints on the petrogenesis of Permian–Triassic Emeishan flood basalts in southwestern China: Lithos, v. 58, p. 145–168.

Yang, H. J., Frey, F. A., Weis, D., Giret, A., Pyle, D., and Michon, G., 1998, Petrogenesis of the flood basalts forming the northern Kerguelen Archipelago: Implications for the Kerguelen plume: Journal of Petrology, v. 39, p. 711–748.

Zhang, Y. X., Luo, Y. N., and Yang, C. X., 1988, Panzhihua-Xichang rift in China: Beijing, China, Geological Publishing House, p. 141–184 (in Chinese with English abstract).

Zhang, Z. C., Hao, Y. L., and Wang, F. S., 2003, Picrites in large igneous provinces and their implications: Earth Science Fontiers, v. 10, p. 105–114 (in Chinese with English abstract).

Zhang, Z. C., and Wang, F. S., 2002, Geochemistry of the two types of basalts of the Emeishan basaltic province: Evidence for mantle plume-lithosphere interaction: Acta Geologica Sinica, v. 76, p. 138–147.

Zhang, Z. C., and Wang, F. S., 2003a, A method for identifying primary magma: Examples from picrite and alkali basalts: Journal of Jilin University, v. 33, p. 130–134 (in Chinese with English abstract) .

Zhang, Z. C., and Wang, F. S., 2003b, Sr, Nd, and Pb isotopic characteristics of Emeishan basalt province and discussion on their source region: Earth Science—Journal of China University of Geosciences, v. 28, p. 431–439 (in Chinese with English abstract) .

Zindler, A., and Hart, S. R., 1986, Chemical geodynamics: Annual Review of Earth and Planetary Sciences, v. 14, p. 493–571.